

MARIA S. MERIAN-Berichte

Geomorphology, processes and geohazards of giant submarine landslides and tsunami generation capacity, as recorded in the sedimentary record of the only historic slide of this kind: the 1929 Grand Banks landslide of the Canadian Atlantic continental margin

Cruise No. MSM47

September 30 – October 30, 2015,
St. John's (Canada) – Ponta Delgada, Azores (Portugal)



S. Krastel

**A. Braeunig, P. Feldens, A. Georgioupolou, H. Jaehmlich,
M. Lange, K. Lindhorst, J. Llopart, S. Mader, L. Mehringer,
M. Merl, I. Muecke, C. Renkl, R. Roskoden, M. Schoenke,
I. Schulten, J.-P. Schwarz, C. Stevenson, M. Vallee, B. Wegener,
L. Wiesenber**

Editorial Assistance:

DFG-Senatskommission für Ozeanographie
MARUM – Zentrum für Marine Umweltwissenschaften der Universität Bremen

2016

The MARIA S. MERIAN-Berichte are published at irregular intervals. They are working papers for people who are occupied with the respective expedition and are intended as reports for the funding institutions. The opinions expressed in the MARIA S. MERIAN-Berichte are only those of the authors.

The MARIA S. MERIAN expeditions are funded by the *Deutsche Forschungsgemeinschaft (DFG)* and the *Bundesministerium für Bildung und Forschung (BMBF)*.

Editor:

DFG-Senatskommission für Ozeanographie
c/o MARUM – Zentrum für Marine Umweltwissenschaften
Universität Bremen
Leobener Strasse
28359 Bremen

Author:

Prof. Dr. Sebastian Krastel
Christian-Albrechts-Universität zu Kiel
Otto-Hahn-Platz 1
24118 Kiel

Telefon: +49 431 880 3914
Telefax: +49 431 880 4432
e-mail: skrastel@geophysik.uni-kiel.de

Citation: S. Krastel, A. Braeunig, P. Feldens, A. Georgioupolou, H. Jaehmlich, M. Lange, K. Lindhorst, J. Llopis, S. Mader, L. Mehringer, M. Merl, I. Muecke, C. Renkl, R. Roskoden, M. Schoenke, I. Schulten, J.-P. Schwarz, C. Stevenson, M. Vallee, B. Wegener, L. Wiesenberg (2016) - Geomorphology, processes and geohazards of giant submarine landslides and tsunami generation capacity, as recorded in the sedimentary record of the only historic slide of this kind: the 1929 Grand Banks landslide of the Canadian Atlantic continental margin - Cruise No. MSM47 – September 30 – October 30, 2015 – St. John's (Canada) – Ponta Delgada, Azores (Portugal). MARIA S. MERIAN-Berichte, MSM47, 55 pp., DFG-Senatskommission für Ozeanographie, DOI:10.2312/cr_msm47

ISSN 2195-8483

Table of Contents

1	Summary	3
2	Participants	5
3	Research Program	6
4	Narrative of the Cruise	9
5	Preliminary Results	15
5.1	Hydroacoustics	15
5.1.1	Bathymetric mapping	15
5.1.2	Sediment Echo Sounding	17
5.1.3	ADCP	23
5.2	High resolution 2D multichannel seismic profiling	24
5.2.1	System components	25
5.2.2	First results of seismic survey	26
5.3	Sediment Sampling	30
5.3.1	Core processing	31
5.3.2	Preliminary coring results	32
5.4	CPT measurements	39
5.4.1	Instrumentation	39
5.4.2	Data acquisition	40
5.4.3	Data processing	43
5.4.4	Preliminary results	43
6	Ship's Meteorological Station	45
7	Station List MSM47	46
8	Data and Sample Storage and Availability	53
9	Acknowledgements	53
10	References	54

1 Summary

On November 18, 1929, a M7.2 earthquake occurred beneath the Laurentian Channel off the coast of Newfoundland. Nearly simultaneously, 12 undersea trans-Atlantic communication cables were severed and within two hours, a devastating tsunami struck the south coast of Newfoundland, claiming 28 lives. Only in 1952, it was understood that a slump-generated turbidity current caused the sequential severance of the cables and likely generated the tsunami. The 1929 Grand Banks events were pivotal, as they led to the first unequivocal recognition of a turbidity current and landslide-triggered tsunami. The landslide site was visited numerous times as underwater survey technologies evolved. No major head scarp related to the event is recognized. The landslide appears to have affected shallow sediments (top 5-100 m) and was laterally extensive. In order to test the hypothesis that a distributed, laterally extensive, shallow submarine mass failure event caused the tsunami, we collected ~ 1500 km of seismic lines in combination with a dense net of hydroacoustic data. A total of ~130 m of gravity cores were recovered at 30 stations. Giant box cores were taken at 15 stations. Three CPT (free-fall cone penetrating testing) transects were collected across landslide scarps.

The data in the failure area show abundant small scarps and several young landslide deposits. The existing bathymetric data were slightly expanded to the shelf break but no obvious major scarp was discovered. The combined interpretation of existing and new data will allow estimating the volume of the failed material, which is an important input parameter for tsunami modelling. Another important aspect will be to assess the activity of listric faults in the failure area with special emphasis on their role for the failure dynamics and the triggering of the tsunami. The deposits of the related turbidity current were investigated in a complex channel area downslope of the failure area. Several coring transects will allow to reconstruct the flow lines of the 1929 turbidity current from bypass-dominated to depositional areas. Very coarse gravel was sampled up to 150 m above the canyon thalweg. First estimates suggest high concentrations of sediments in the flow, which was able to run out over 1000s of kilometers.

Zusammenfassung

Am 18.11.1929 erschütterte ein Erdbeben der Stärke M7.2 den Bereich des Laurentian Channels vor der Küste Neufundlands. Fast zeitgleich wurden 12 transatlantische Unterseekabel beschädigt; innerhalb von 2 Stunden wurde die Südküste Neufundlands von einem zerstörerischen Tsunami getroffen, der 28 Menschenleben forderte. Erst im Jahr 1952 wurde verstanden, dass ein Slump und/oder Turbiditstrom die Ursache für das sequentielle Brechen der Unterseekabel und vermutlich auch für den Tsunami war. Das 1929 Grand Banks Ereignis ist von zentraler Bedeutung, da es die erste eindeutige Dokumentation eines rutschungsinduzierten Tsunamis ist. Das Gebiet wurde mit fortschreitender Messtechnik mehrfach untersucht. Eine große Abrisskante konnte bisher nicht identifiziert werden. Die Rutschung scheint nur flache Sedimente (5-100m) auf einer sehr großen Fläche betroffen zu haben. Um die Hypothese zu testen, dass eine flache aber räumlich ausgedehnte Rutschung den Tsunami ausgelöst hat, haben wir 1500 km

hochauflösende seismische Daten in Verbindung mit einem engen Netz aus hydroakustischen Daten aufgezeichnet. Insgesamt wurden mittels Schwerelot 130 m Sediment an 30 Stationen gewonnen; Großkastengreifer wurden an 15 Stationen eingesetzt. 3 CPT-Profile (free-fall cone penetrating testing) wurden über unterschiedliche Abrisskanten gesammelt.

Die Daten im Bereich des Hangversagens zeigen zahlreiche kleinere Abrisskanten und junge Rutschungsablagerungen. Die bestehende Überdeckung mit bathymetrischen Daten wurde bis zur Schelfkante ausgeweitet, aber auch dort wurden keine größeren Abrisskanten identifiziert. Die kombinierte Analyse der existierenden und neuen Daten wird es ermöglichen, das Volumen des Rutschungsmaterials abzuschätzen, was ein wichtiger Input-Parameter für Tsunami-Modellierungen ist. Weiterhin wird es möglich sein, die Aktivität von listrischen Verwerfungen zu analysieren, die eine wichtige Rolle für die Dynamik des Hangversagens und damit auch für die Initiierung des Tsunamis haben können. Die Ablagerungen des Turbidites von 1929 wurden intensiv in einem komplexen Kanal-System unterhalb der Abrisskanten untersucht. Mittels mehrere Kernprofile werden wir die Konzentration und die Höhe des Turbiditstroms von Bypass-dominierten zu Ablagerungs-dominierten Gebieten rekonstruieren können. Grobe Kiese wurden noch bis zu 150 m oberhalb des Canyon-Bodens gefunden. Erste Abschätzungen deuten auf hohe Sedimentkonzentration im Turbiditstrom hin, der sich mehr als 1000 km ausgedehnt hat.

2 Participants

Name	Discipline	Institution
Krastel, Sebastian, Prof. Dr.	Chief Scientist	CAU
Lindhorst, Katja, Dr.	Seismics/Hydroacoustics	CAU
Bräunig, Anja	Seismics/Hydroacoustics	CAU
Mader, Sarah	Seismics/Hydroacoustics	CAU
Merl, Maximilian	Seismics/Hydroacoustics	CAU
Muecke, Isabell	Seismics/Hydroacoustics	CAU
Wiesenbergs, Lars	Seismics/Hydroacoustics	CAU
Schulten, Irena	Seismics/Hydroacoustics	BIO
Valle, Maxlimer	Seismics/Hydroacoustics	UNH
Renkl, Christoph	Seismics/Hydroacoustics	DAL
Jähmlich, Heiko	Technician	CAU
Georgiopoulou, Aggeliki, Dr.	Sedimentology	UCD
Stevenson, Christopher, Dr.	Sedimentology	UoL
Schönke, Mischa	Sedimentology	CAU
Schwarz, Jan-Philipp	Sedimentology	CAU
Feldens, Peter, Dr.	Geotechnics/Sedimentology	IOW
Wegener, Babette	Geotechnics/Sedimentology	IOW
Llopert, Jaume, Dr.	Geotechnics/Sedimentology	CSIC
Roskoden, Robert	CPT	MARUM
Mehringer, Lisa	CPT	MARUM
Lange, Matthias	Technician	MARUM

BIO	Bedford Institution of Oceanography, Dartmouth
CAU	Christian-Albrechts-Universität zu Kiel
CSIC	Institut de Ciències del Mar
DAL	Dalhousie University, Halifax
IOW	Institut für Ostseeforschung, Warnemünde
MARUM	Zentrum für Marine Umweltwissenschaften, Bremen
UCD	University College Dublin
UNH	University of New Hampshire
UoL	University of Leeds

3 Research Program

Within the last two decades, it has come to be understood that sediment mass wasting (submarine landsliding) is a common sedimentary process that plays a major role in construction of continental margins. Evidence of this process is ubiquitous along almost all continental margins; passive, active and transform, as attested (among others) in the many studies that appear in the “Submarine Mass Movements and Their Consequences” volumes of the Advances in Natural and Technological Hazards Research series (supported by UNESCO IGCP projects, e.g. Mosher et al., 2010; Yamada et al., 2012; Krastel et al., 2014; Lamarche et al., 2016).

Also within the last two decades, the World has observed a number of devastating tsunamis. In each case, the tsunamis were coincident with a major earthquake. The question has been posed as to whether or not submarine landslides were the cause or contributed to these tsunamis (Tappin et al., 2001; 2008; Mosher et al., 2009; Harbitz et al., 2014). In the case of the 1998 event at Papua New Guinea, Tappin et al. (2001) believed the tsunami, which resulted in the deaths of over 2000 people, was a direct result of a submarine landslide, despite the fact that there was not clear evidence of a slide from bathymetric records. Wave heights, directions and arrival time were all factors in this conclusion. In the case of the 1929 Grand Banks event, the tsunami struck the coast of Newfoundland about 2 hours following a M7.2 earthquake (Bent 1995). After the event, 12 telecommunication cables were sheared with successive timing, providing direct evidence of submarine sediment mass failure. 28 people were killed by the tsunami.

Hence, the 1929 Grand Banks event was the first proven evidence of the natural occurrence of turbidity currents, through the severing of underwater cables. Most submarine landslides are thought to have been triggered by earthquakes and it is speculated (and supported by numerical simulations) that rapid displacement of sediment by underwater mass failure can generate tsunamis. The 1929 event, however, is still the only clearly documented occurrence of an earthquake-generated submarine landslide that resulted in a tsunami. This fact alone makes it worthwhile to study the details of the geology concerning this event in order to understand the processes and to recognize conditions elsewhere in the World that may lead to similar styles of failure with similar consequences. Available data in the Grand Banks region show small escarpments (~20 m vertical) throughout the region, some of which may have been created in the 1929 event. Remarkably, the seafloor imagery is not different than other regions of the Nova Scotian margin or than many continental margins around the globe for that matter. In other words, there is no evidence of a major submarine landslide scar or deposit - such as the Storegga Slide off Norway. This paradox leads to a number of research questions.

What are the dimensions of the failed material (area and volume) recognized in surficial sediments?

These data are needed as input for numerical simulations of tsunami generation; the more accurate the metrics, the more realistic the simulation. Multibeam bathymetric, subbottom profiler and high resolution seismic reflection data were collected to address this question.

What are the geologic / geotechnical processes of failure?

The speed of initial failure is critical for model inputs. The thixotropic properties of the sediment are key to the initial speed of failure and behavior of the flow during the failure process. To answer these questions, initial and post-failure geotechnical conditions of sediment were measured, including in situ testing by cone penetrating testing (CPT). In addition, interpretation of seismic profiles and seismic geomorphology of deposits will provide controls on failure styles (e.g. translational landslide vs debris flow vs turbidite). We acquired densely spaced 2D seismic reflection data for answering this question.

What are the properties of the sediment prior to failure, i.e., what are the preconditioning factors that made the sediment susceptible to failure in the earthquake?

These factors are necessary to understand the failure process and recognize potential failure conditions elsewhere. Similar data to above has been collected especially from areas, which have not failed yet.

What are deeper structural controls? Are there faults, stratigraphic factors (unconformities, decollements), underlying salt bodies, and or gas hydrate that contributed to the mass failure?

Structural controls are often ignored in the study of surficial processes, but they are critical to mass failure, supplying pre-conditioning factors and propagating ground accelerations in an earthquake. High resolution and multi-channel seismic reflection profiles were collected in order to address this question.

Can the documented surficial failures generate a tsunami? If so, at what stage in the failure process would the tsunami be generated?

The failure was shown to be shallow and widespread and rapidly deteriorated into a confined turbidity current that moved at great speed down channels of the Laurentian Fan. It is unknown if this failure style is capable of generating a tsunami in water depths of 500 to 2500 m, or if the turbidity current could in any way contribute to tsunami generation. Sophisticated numerical simulation of failure, water column coupling and tsunami generation and propagation are required for these questions. Data for determining input parameters were collected during the cruise

What is the frequency of these types of failure?

The geologic record shows evidence of multiple failure events throughout the stratigraphy. The frequency of occurrence applies directly to risk assessment, but also alludes to triggering and contributing factors. Seismic reflection profiles and correlation to industry wells for age control are required to answer such a question.

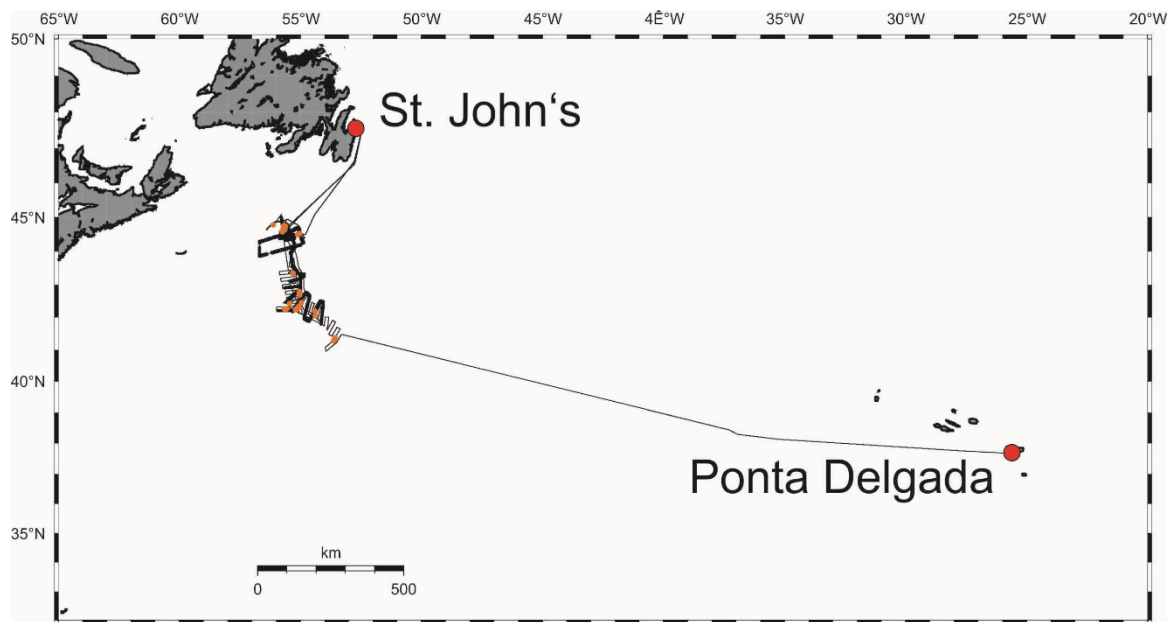


Fig. 3.1 Cruise track of Cruise MSM47. Details of the working area are shown in Figs 05 and 08.

Methods

The main methods used during Cruise MSM47 are the hydro-acoustic systems of RV MARIA S. MERIAN (Multibeam, PARASOUND, ADCP), high-resolution multichannel reflection seismics, gravity/giant box coring and CPT (Cone penetration Testing) measurements. The high-resolution seismic system consisted of two GI-Guns and a 176-channel 275 m-long digital Geometrics GeoEel streamer. This system is optimized for collecting high-resolution seismic data, which allows resolution of small-scale sedimentary structures and closely spaced layers on a meter scale, which usually cannot be resolved by means of conventional seismic systems. On the other hand, the high number of channels and the usage of two GI-Guns allowed sufficient penetration even in great water depths. The deep-water cone penetrometer (CPT) probe was deployed by winch in pogo-style, i.e. it is profiling the uppermost meters of the sediment dynamically and measures the strength and pore pressure of the strata (the latter value being extrapolated after approx. 20 mins of dissipation at each location). Standard gravity and giant box corers were used for geological sampling. Hydroacoustic data were collected by means of systems installed on RV MARIA S. MERIAN.

We started with regional seismic overview profiles in order to map the margin structure in and outside the failure area (Fig. 3.1). Thereafter work was carried out in two areas (Figs 05 and 08). Area 1 (northern area) is the main failure area of the initiation of the 1929 Grand Banks landslide. Hydroacoustic (including multibeam) data were already available for this area. The main focus in Area 1 was on seismic imaging, targeted coring and CPT deployments. Area 2 is the seaward extension of Area 1 (southern area, lower St. Laurentian Fan). Data coverage in this area was sparse. Hence, we started with hydroacoustic mapping

(especially multibeam), followed by seismic imaging, and coring. Coring locations were chosen based on the new acoustic data.

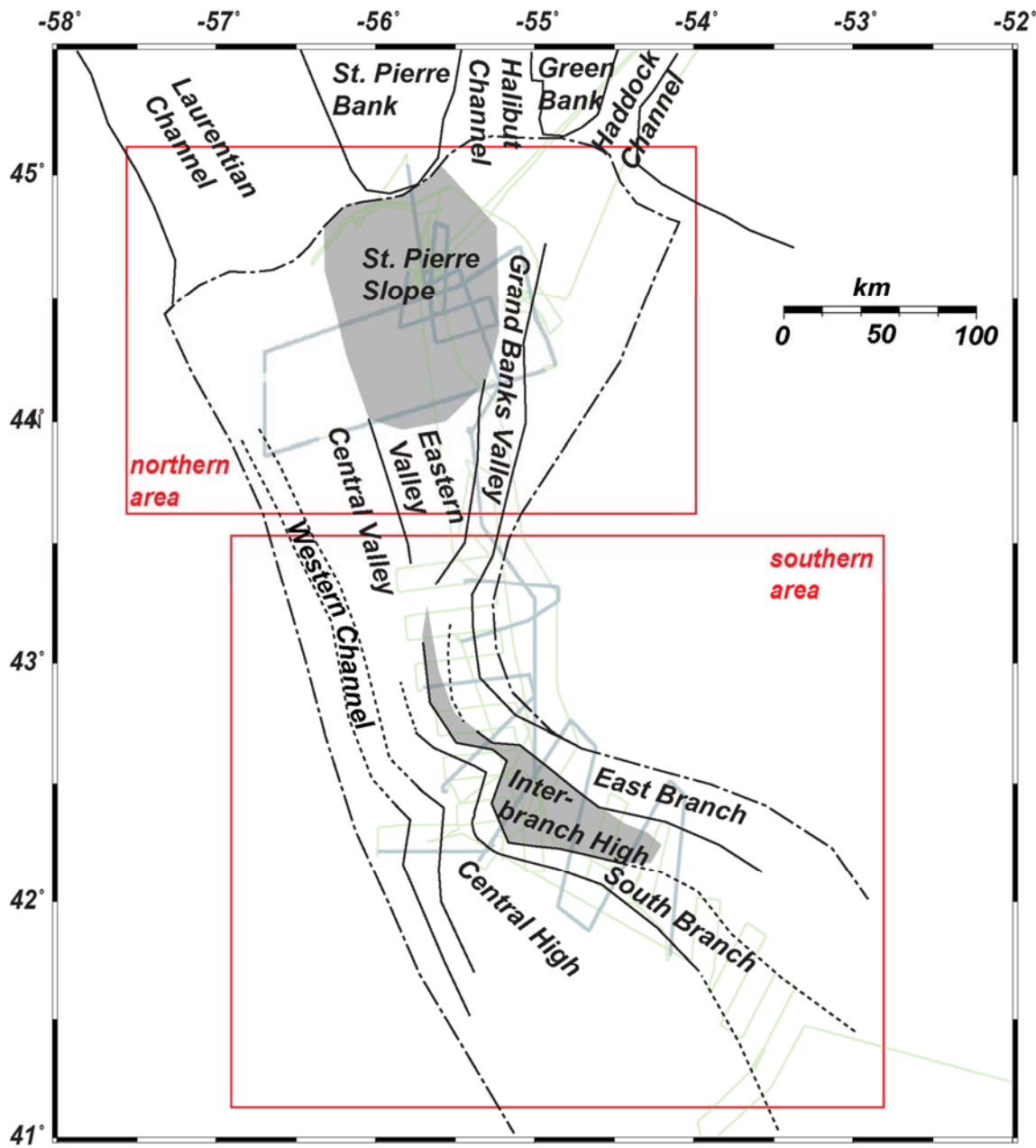


Fig. 3.2 Nomenclature of morphological structures within the study area (modified after Clarke et al., 1990).

4 Narrative of the Cruise

The scientific party arrived in St. John's on September 28th and 29th. All science team members boarded RV MARIA S. MERIAN on the 29th. RV MARIA S. MERIAN left the port of St. John's on September 30th at 16:00h after bunkering at very pleasant weather conditions (sunny skies and calm seas). During departure, we had some spectacular views of the Newfoundland coastline.

The scientific crew of Cruise MSM47 included 10 scientists from the Christian-Albrechts-Universität zu Kiel, 3 scientists from the MARUM (Bremen University), 2

scientists from the Baltic Sea Research Institute (Warnemünde), and one scientist each from Bedford Institute of Oceanography (Dartmouth), Dalhousie University (Halifax), University College Dublin, the University of Leeds, the Institut de Ciències del Mar Barcelona, and the University of New Hampshire. The transit in the working area was very short and the scientific program started on October 1st at 02:00h local time with switching on the hydroacoustic systems. We headed to the eastern flank of the Grand Banks Valley in order to collect a sound velocity profile (SVP) for the multibeam systems and for taking a first gravity core followed by a CPT deployment. Based on the PARASOUND data, we chose a location with good penetration about 500 m above the thalweg of the Grand Banks Valley (Station MSM47_01). The SVP deployment worked without any problems. The first 6 m long gravity corer over penetrated and a second longer core brought up 810 cm of sediments. Several drop stones as well as undisturbed shells and shell fragments were found in the core. The gravity corer showed an interlayering of greenish and reddish sediments with quite some bioturbation. The reddish layers show a very sharp partly erosive contact at their base and are interpreted as turbidites. They most likely originate from the St. Pierre Slope, where reddish sediments are widespread while the greenish sediments represent the sediments deposited east of the Grand Banks Valley. A prominent sand layer in ca. 50 cm sub-bottom depth is clearly visible in the core. This layer is mechanically weak, which was confirmed by a CPT deployment at the same location. The seismic equipment was deployed immediately after station work was finished in the evening of October 1st. We started with two long slope parallel profiles in order to characterize the general setting of the wider working area. Unfortunately, wind speed picked up significantly on October 3rd (gusts up to beaufort 8) but the sea state still allowed to continue the seismic survey though noise levels increased significantly. The seismic equipment was recovered on October 4th at 07:00h. The data showed that the western part of the proposed failure area has not significantly contributed to the landslide allowing us to focus on the central working area. October 4th was used to sample lower terraces near core MSM47_01. A short hydroacoustic survey showed a terrace only about 20 m above the thalweg. A box-corer (MSM47_02), however, was almost empty and hence we moved one terrace further up (MSM47_03, ~80 m above the thalweg). Recovery in the box-corer was again very low. The sediments were very stiff. The box corer was followed by a gravity corer, which resulted in 256 cm recovery of very stiff greenish sediments. It seems that the turbidity currents were purely erosive at this location and have not left any deposits behind.

We deployed the seismic gear around 19:00h in the evening of October 4th but quickly realized that the sea state was too rough for collecting seismic data. Hence, we changed plans and started a hydroacoustic survey of the shelf break in order to check for scarps close to the shelf break. The distal deposits of the Grand Banks landslide are known to contain coarse sands and gravel; the shelf break is a potential source of such material. The survey showed several scour marks of icebergs and small failures but no major scarps. The survey was not including the French EEZ of St. Pierre, because entry to the French EEZ needed to be announced well in advance (usually 36h).

October 5th was a good coring day across a prominent 20-30 m high morphological step at a mid-slope position. The hydroacoustic data indicated young debrite deposits beneath

the morphological step. The first station targeted the distal deposits of the debrites (Station MSM47_04). A box corer showed very thin (~4 cm) soft sediments on top of a muddy debrite. The base of the debrite was sampled with a gravity corer, which is a promising target for geotechnical work. The second core (MSM47_05) targeted background sediments. Total recovery was 787 cm but the core also contains some debrite deposits in the upper 1.5 m. A re-assessment of the PARASOUND data indeed showed a very thin debrite lobe at this location.

The seismic gear was deployed after coring on October 5th at 21:00h. We shot two lines crossing proposed listric faults in a mid-slope position. One hypothesis for the tsunami generation during the 1929 event proposes movement along these faults as major contribution to the tsunami. Detailed analysis of all available seismic profiles across these faults is needed for assessing their importance for the tsunami generation. Two additional stations were sampled on October 6th slightly above the morphological step at the mid-slope location. Both cores (MSM47_06 and 07) targeted debris tongues, which were successfully sampled.

Station work had to be interrupted on October 6th at 18:42h local time (20:42 UTC) due to a medical evacuation of one scientist. We were heading full speed to the port of St. John's where we arrived on October 7th at 13:00h local time (15:00h UTC). We left port again already at 13:48h local time (15:48h UTC) and headed back to the working area. We continued our program on October 8th at 08:06h local time (10:06h UTC) with a short hydroacoustic survey in order to define final locations for a CPT transect across a headwall in about 1800 m water depth. This transect started around 10:00h (Station MSM47_08). We had to stop the profile around 18:00h because the battery of the CPT was empty. The night was used to collect two along slope seismic profiles in an area, which was only sparsely surveyed with airgun seismics before. The seismic gear was retrieved on October 9th around 9:00h. Afterwards we continued the CPT transect, which was interrupted the day before (Station MSM47_09). For a better understanding of the distribution of the debrite identified in the previous cores, we headed upslope in order identify the origin of the widespread debrite. Another set of prominent scarps is found in ~1000 m water depth. The debrite can be easily traced to these scarps based on hydroacoustic profiles but correlation becomes tricky upslope of the scarps. Hence, we took a giant box core and a gravity core (MSM47_10, 768 cm recovery) upslope of the scarps in an area, which looks undisturbed. The core is indeed undisturbed. Hence, the scarp area in about 1000 m water depth was formed recently or was at least reactivated recently, possibly during the 1929 event.

Another short CPT transect targeting different debrite lobes was collected in the evening of October 9th (MSM47_11). The rest of the night was used for mapping the shelf break in the French EEZ. We can now exclude a major failure of the shelf break as source for the 1929 landslide based on our new data. A large number of small and very fresh looking scarps are found beneath the shelf break in about 700 m water depth. We took a core beneath one of these scarps (MSM47_12) in the morning of October 10th. We sampled debrite deposits but the debrite is overlain by about 250 cm of background sediments indicating that these failures are much older than the 1929 event.

On October 10th at 13:00h, we started to collect a long seismic profile to the southern working area, where indications of the deposits of the 1929 event have been reported before. Around noon on October 11th, one of the airguns stopped shooting due to a break in a firing line. As repairs took a bit longer, we continued with hydroacoustic mapping. The focus was a postulated bifurcation point of the Eastern Channel. This bifurcation point was reconstructed based on single beam echo sounder profiles; bathymetric mapping showed that no bifurcation point exists at the proposed location but two separate channels.

A first core in the southern working area was taken on October 12th in the morning on an outer bend of the southern branch of the mapped channels in about 4440 m water depth (Station MSM47_13). A gravity corer was filled with 775 cm of sediments. The upper most part (ca. 1 m) showed a strange succession of relatively stiff sediments on top of homogeneous greyish sediments. The greyish unit is underlain by reddish mud with a large number of spill over turbidites. Coring was followed by a seismic survey across different sections of the channel system beneath the postulated bifurcation point of the Eastern Channel. Seismic surveying was continued until October 14th around 17:00h.

A gravity core of the channel thalweg (MSM47_14) of the southern branch of the channel was taken in the evening of October 14th. The backscatter data showed relatively low values indicating potentially soft sediments at the seafloor. However, the gravity corer bounced at the seafloor. A bit of silty sediments were found at the weight of the gravity corer. The night was used for further mapping of the channel system. Based on the available maps, two stations were sampled on October 15th. Both stations were located at the morphological high beneath the two channel branches visible in the bathymetric data. Both cores (MSM47_15 and 16) show a very thin soft sediment layer on top of stiff sediments. A small sand layer was found between the fluffy surface sediments and the stiff sediments beneath. The night was used for further hydroacoustic mapping. During this mapping, we provided the final proof that the bifurcation point does not exist at the proposed location but further upslope. October 16th was used for further coring. The first gravity core (MSM47_17) was taken on a terrace about ~200 m above the thalweg of the northern branch of the channel. This core bounced but some sand was found on the core barrel. Hence, we moved to a location, which was about 100 m higher above the thalweg compared to the previous station (MSM47_18). This core showed the meanwhile well-known succession of sediments including relatively stiff surface sediments and abundant turbidites of varying color. However, no major sandy turbidite was found close to the surface. Hence, we took another core between the two previous cores (MSM47_019). This core bent but still included 190 cm of sediments. A massive (~30 cm) sandy turbidite was found close to the surface, but it seemed to be overlain by ~10 cm of undisturbed sediments. It is, therefore, unlikely that it represents the 1929 event. Another core was taken at an elevated area, which looks fully undisturbed (MSM47_020). The core had a length of 770 cm and shows a remarkably similar succession of sediments of reddish turbidites in the lower part, interlayered reddish and greenish turbidites in the middle part, which are overlain by bioturbated undisturbed sediments. A thin soft layer with a different color was found on top of the bioturbated sediments. This thin layer was identified in other cores as well and caught our attention. We noted that i) it is overlying sediments, which show a clear

oxidation front but the soft surface layer shows very different colors, ii) it usually has an erosive contact to the underlying sediments and iii) it contains material clearly coming from an shelf/upper slope environment (e.g., angular sand grains, glauconitic). Hence, we interpret this unit as deposits of the 1929 event. The deposits are mainly characteristic for a bypass facies; this facies is very widespread in the working area.

Coring was followed by two additional reflection seismic profiles across the channels. The seismic data suggest that the locations of the channels are structurally controlled. The seismic was retrieved on October 17th in order to map the channels at higher speeds with the hydroacoustic systems. This mapping showed that the channels merge further upslope. Mapping was completed on October 18th in the early morning. The day and the following night was used to continue the seismic profile connecting the northern and southern working area, which was interrupted earlier during the cruise. Seismic profiling was continued until October 19th early morning. We planned to take a coring transect across the Southern Channel at different heights above the thalweg on October 19th. We started with a box corer (MSM47_21) about 170 m above the thalweg. Unfortunately, the box corer did not trigger. In the following gravity corer, we sampled a ~20 cm thick fluffy layer right at the surface representing a soupy graded turbidite sand to sandy mud. This unit is thicker than at previous locations. This is consistent with our interpretation of these deposits as 1929 turbidite. A second core (MSM47_22) was located on a small terrace just 80 m above the thalweg in an inner bend. The core bent but gravel was found in the core catcher. Hence, the coarse-grained part of the 1929 turbidite had a height of at least 80 m. At this point, we had to terminate coring activities due to strong winds.

We started a long line filling in gaps in the bathymetry to the northern working area because wind conditions were forecasted to be better further to the north for the next day. We arrived at a morphological step interpreted as headwall in the early morning of October 20th. A core (MSM47_23) was taken in a transparent layer interpreted to be debrite based on the hydroacoustics data. The core showed debrite deposits but they are covered by undisturbed hemipelagic sediments; hence, the debrite is not very young. Another core (MSM47_24) was taken upslope of the morphological step at an almost identical location as Core MSM47_10, which sampled undisturbed deposits. We planned to duplicate Core MSM47_10 for geotechnical measurements but had to move the location slightly to the east due to fishing activities in this area. Coring was followed by a CPT-transect across the morphological step. Two additional cores were taken afterwards. The first core was taken upslope of cores MSM47_06 and 07, and this core (MSM47_26) showed again debrite deposits close to the surface proving that the morphological step in about 900 m water depth was at least partially reactivated in the recent past. A second core was a duplicate of Core MSM47_04 for geotechnical measurements.

The night was used for a transit to an area slightly downslope of the joining point of the Grand Banks Valley and the Eastern Channel. PARASOUND profiles showed promising coring locations at this location. A first gravity core about 250 m above the thalweg bounced but a box core recovered coarse sand and gravel without a drape (MAM47_27). A gravity core 20 m further up at greater distance to the channel (MSM47_28) recovered almost 5 m of sediments with the same turbidite recovered at the box corer but background

sediments beneath. Coring was followed by seismic reflection profiling until early morning of October 22nd. We collected two long slope parallel profiles for stratigraphic work at the lower slope. October 22nd was an intense coring day (Cores MSM47_29 -32). These cores completed a transect across the Southern Channel. Varying deposits of the 1929 event were sampled at different heights above the channel thalweg, allowing to reconstruct the trim line of the 1929 event.

In order to estimate the importance of the Western Channel, we collected a seismic line and additional hydroacoustic data of the Western Channel during the night and the morning of October 23rd. Landsliding of the channel walls is extremely widespread at the Western Channel. The seismic data show thick debrite deposits at the channel floor. We took a first core at a terrace about 100 m above the thalweg of the Western Channel (MSM47_33), which allowed us to sample the 1929 turbidite. A box corer from the channel thalweg (MSM47_34) was similar to a box corer of the Southern Channel.

In order to characterize the boundary from mainly bypassing through depositional, we mapped the Southern Channel further downslope. The channel spreads over a larger area with increasing water depth and flow structures become visible on the backscatter map. We tried to collect another coring transect in the night to October 25th at relatively rough weather conditions. A box corer from the channel thalweg (MSM47_35) did not trigger. A first gravity core (MSM47_36) on the southern channel margin penetrated into the sediments but the core catcher was sheared-off, most likely due to a large boulder. The corer bounced at this location in a second try. Core MSM47_37 was taken a bit further away from the channel axis. The core bounced as well but contained ~40 cm of coarse gravel documenting deposition of the turbidite in this area. A seismic profile was planned for the day but the sea state was too rough for deploying the seismics; hence, we collected additional hydroacoustic data. We started our transit to Ponta Delgada at 16:42 h local time on October 25th, which was the end of the research program of Cruise MSM47. We used the long transit for preliminary data processing and interpretation having all the experts onboard. Plans for future investigations and detailed work on collected data were made. We arrived in Ponta Delgada at 08:50h local time on October 30th.

RV MARIA S. MERIAN-Cruise MSM47 was a great success, despite the fact that we lost about 1.5 days due to a medical evacuation. Weather was reasonable and research activities were always possible though we frequently had to adjust our program to the weather conditions. In summary, we collected about 1500 km of seismic 2D-lines in exceptional quality. Hydroacoustic data were collected during designated surveys as well as along all seismic profiles and transits (total of ~5000 km); widespread previously unknown areas were mapped. We collected gravity cores at 30 stations with a total core length of 130 m. We took box cores at 15 stations. Coring was not always easy due to the thick widespread sandy base of the 1929 turbidite but we managed to sample and characterize the 1929 Grand Banks landslide and turbidite from a bypassing region to its more depositional part. Two cores were duplicated for geotechnical measurements. Additional geotechnical data were collected along 3 CPT transects. The new data will allow an in depth investigation of the morphology, processes and geohazards of the Grand Banks area including the tsunami generation capacity of the 1929 Grand Banks landslide.

5 Preliminary Results

5.1 Hydroacoustics

5.1.1 Bathymetric mapping

(P. Feldens, K. Lindhorst, A. Bräunig, S. Mader, M. Merl, I. Mücke, C. Renkl, I. Schulten, M. Vallee, L. Wiesenberge)

Technical description

During Cruise MSM47, the hull-mounted Kongsberg Simrad system EM122 was used for bathymetric mapping. The deep water system EM122 was operated continuously in a 24-hour schedule. Several surveys were especially designed for collecting multibeam data. The EM122 system allows an accurate bathymetric mapping down to full ocean depth. Basic components of the system are two linear transducer arrays in a Mills cross configuration with separate units for transmitting and receiving.

The nominal sonar frequency is 12 kHz with an angular coverage sector of up to 150° and 864 soundings per ping. The EM122 has a dual swath capacity, hence one ping consists of two swathes of up to 432 soundings each. The dual swath capacity increases the along track resolution of the multibeam data. The typical depths in our investigation area are between 500 and 5000 m water depth, allowing spacing bathymetry grid resolution of about 30 m to 200 m across and along, given survey velocities between 4.5 and 12 kn. The achievable swath width on a flat bottom will normally be up to six times the water depth. However, we limited the swath width to 15 km and 65° in order to guarantee good resolution in across track direction in deep water.

The angular coverage sector and beam pointing angles may be set to vary automatically with depth according to achievable coverage. This maximizes the number of usable beams. The beam spacing was set to equidistant. Using the detected two-way-travel-time and the beam angle known for each beam, and taking into account the ray bending due to refraction in the water column due to sound speed variations, depths are calculated for each beam. A combination of amplitude (for the central beams) and phase (slant beams) is used to provide a measurement accuracy practically independent of the beam pointing angle. Beside the depth values, the EM122 provides also backscatter information and pseudo-side-scan images as well as water column imaging (WCI) capabilities. WCI data were recorded for a large part of the survey, but were not recorded continuously. Preliminary bathymetric and amplitude grids were created using the MBSYSTEM software. Preliminary processing included general quality checks (navigation, attitude data, sound velocity profiles), the generation of a surface, the correction of angular effects on backscatter strength and the conservative automatic removal of spikes and turns. All grids and images created during this cruise are stored in geographic coordinates with the WGS84 ellipsoid. All data were imported in the Global Mapper software. A map of available bathymetric data collected during MSM47 and short descriptions of different morphological features are given on Figs Fig. 5.3 and 09.

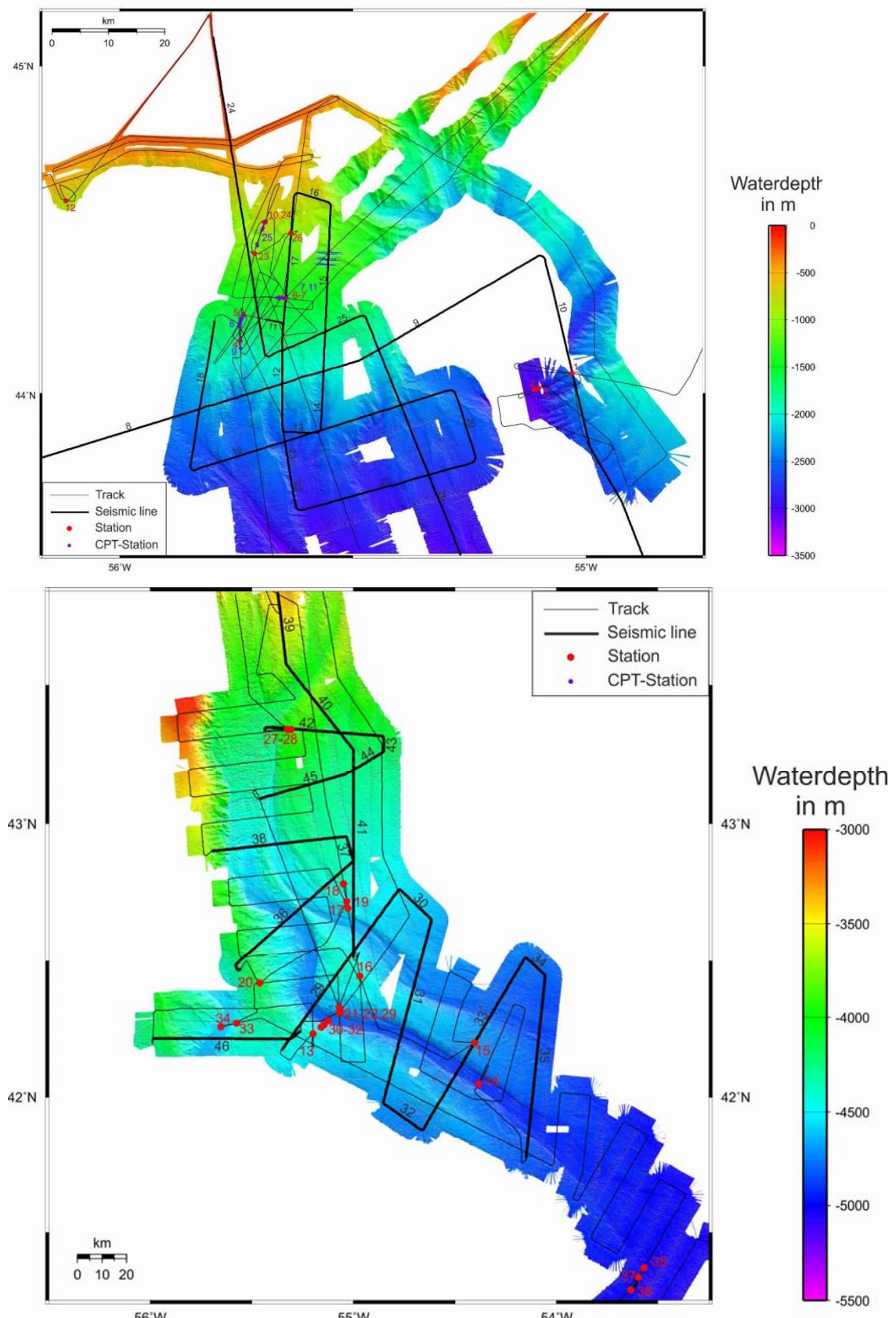


Fig. 5.3 Track plots of the working areas (top: North, bottom: South) together with recorded bathymetry. Red number correspond to geological stations. Black numbers show line number of seismic profiles. Blue numbers are CPT Transects.

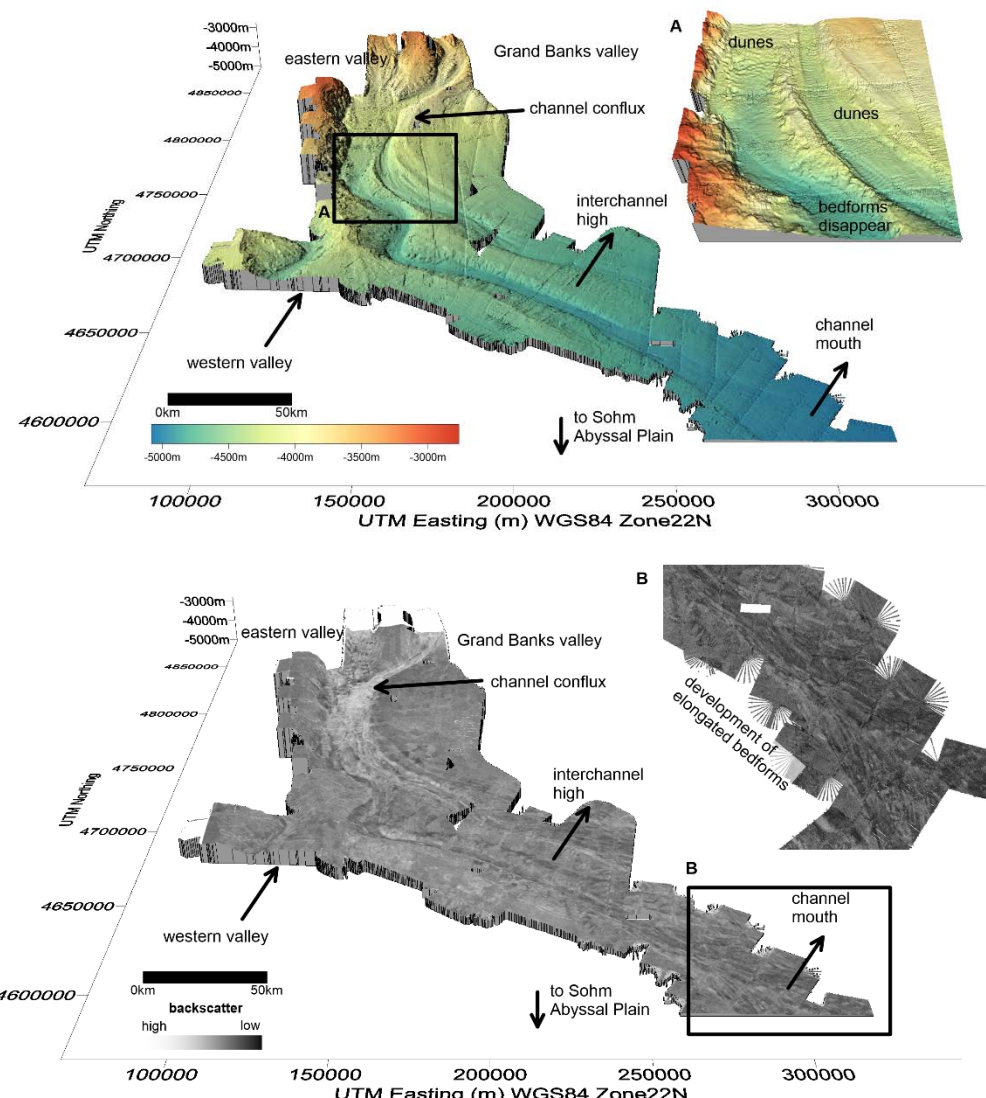


Fig. 5.4 Bathymetric data (top) and backscatter data draped on top of bathymetry (bottom) of the southern investigation area. In the bathymetric data, the conflux of the Grand Bank valley and the Eastern valley is observed. The channels are quickly separated again by an interchannel high. Interestingly, bedforms develop only in the Central Valley, while a smooth seafloor is observed in the south. This is reflected in the backscatter data, where typical high backscatter intensities are only observed above the conflux of the channels and to the north of the interchannel high. The majority of the channel south of the interchannel high shows low backscatter intensities, with the exceptions of the inner bend slopes. Near the channel mouth, the development of elongated bedforms with alternating high and low backscatter intensities is observed.

5.1.2 Sediment Echo Sounding

(K. Lindhorst, A. Bräunig, S. Mader, M. Merl, I. Mücke, C. Renkl, I. Schulten, M. Vallee, L. Wiesenbergs)

System description

The Atlas PARASOUND system P70 uses the parametric effect, which occurs when very high (finite) amplitude sound waves are generated. If two waves of similar frequencies are generated simultaneously, also the sum and the difference of the two primary frequencies

are emitted. For the PARASOUND System, 18 kHz is one fixed primary frequency, which is generated by a transducer of ~ 1m length within a beam of 4.5°. The second primary frequency can be varied between 18.5 and 24 kHz, resulting in difference frequencies from 0.5 to 6.0 kHz. This signal travels within the 18 kHz beam, which is much narrower than e.g. a 4 kHz signal, emitted from the same transducer directly (30°). Therefore, a higher lateral resolution can be achieved, and imaging of small-scale structures on the sea floor is superior to conventional systems. As another consequence, the signal bandwidth is also increased, and much shorter signals can be generated with improved vertical resolution. Due to the narrow beam, it is necessary to control beam direction, to compensate the ship's movement, and to send the energy vertically downwards. The system treats three signals separately: the primary high frequency signal (18 kHz; PHF), the secondary low frequency signal (selectable 0.5 to 6.0 kHz; SLF) and the secondary high frequency (selectable 36.5 to 42 kHz; SHF). We selected 4 kHz as SLF and 40 kHz as SHF.

The PARASOUND system uses a minimum of three different computer systems. Two of them control real-time signal generation and data acquisition through a Linux and a Windows system. The third PC is available for the operator. This Operator-PC hosts the Hydromap Database Server, the Hydromap Control Software and the ParaStore 3 Software. The Hydromap Control Software is responsible for all system settings and for communication with the real-time computers. The ParaStore Software Package is used for visualization, online processing, and data storage. Data can be stored in the PARASOUND ASD format, but also in the more common PS3 or SEG-Y formats. Several windows can be opened to display different signals (PHF, SLF, SHF) with different scaling and/or processing parameters. This allows optimizing the windows for specific purposes, as e.g. imaging of the upper 20 m of sediments to select optimal coring locations, to choose a full penetration plot, which also allows coverage of the topography, or to study the complete water column. The system can be used in the single pulse mode, when a single pulse is emitted and the water column and sediment response are recorded before the next pulse is sent, or in the pulse train or quasi-equidistant mode, by which the two-way travel time of the signal in the water column is used to emit additional signals. Depending on water depth, the signal density can be increased by as much as a factor of 16. We operated the system mainly in the quasi-equidistant mode, which worked very well during the cruise. Raw ASD data were collected for the PHF, SHF, and SLF signal. In addition, we recorded PS3 data of the PHF and SHF signals over a time window between 200 m and 300 m. The PHF depth was used as system depth for most of the time. The system worked very reliable during the cruise and we only had a very small number of system crashes. Data gaps are therefore small. PS3 data for the SLF data were converted to SGY-data covering one profile or 2h – 4h using the software ps32sgy (Hanno Keil, Bremen University). This data were then loaded to IHS Kingdom for immediate analysis of the data especially in order to select coring locations.

Preliminary results:

PARASOUND data were recorded along all seismic profiles and on all transits. A few examples are shown in the following. A PARASOUND line along the southern end of the St. Pierre Slope and then crossing the Grand Banks Valley is shown in Fig. 5.5. On its northern end, a ~30 m thick transparent unit indicates a major sliding event. Sediments deposited on top are affected by the irregular surface of the slide deposits. South of the slide deposits, the sediments are well stratified and reflectors can be traced over long distances. Seismic reflectors are cut at both sidewalls of the Grand Banks Valley. A distinctive double reflector appears to be on both sides of the canyon. The valley itself is filled by sand and eroded material from its sides.

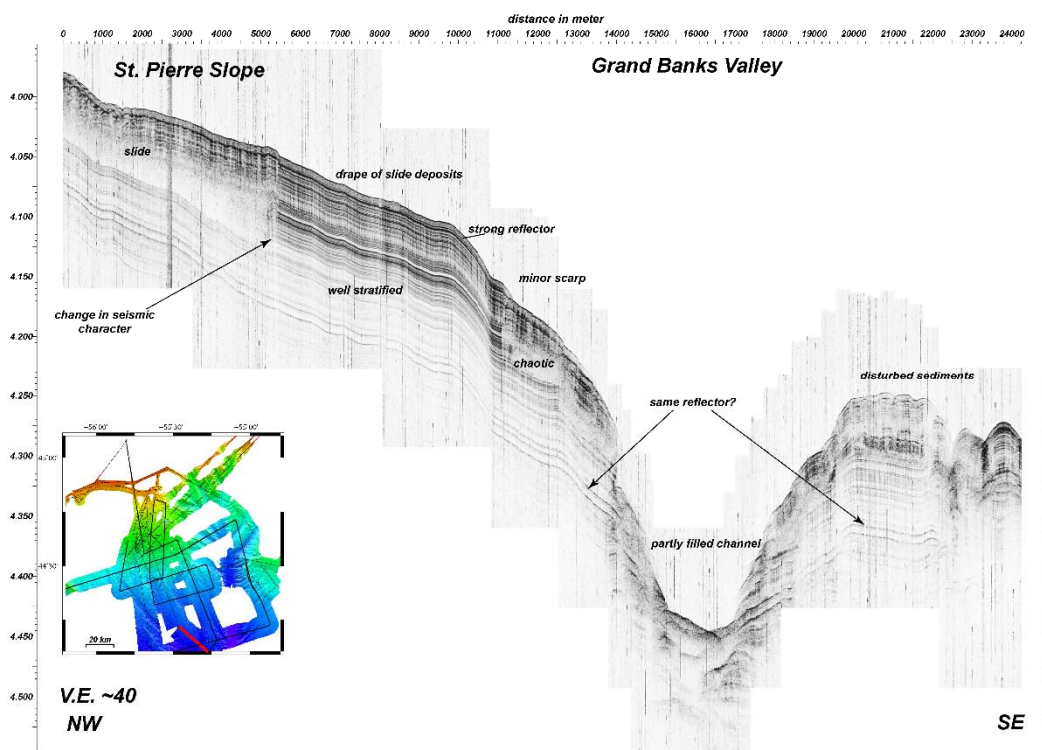


Fig. 5.5 PARASOUND profile imaging typical features of the St. Pierre Slope (NW) and the Grand Banks Valley. See inset map for location of profile.

Figure 11 shows a PARASOUND line crossing the central part of the canyon system in the southern working area, where two channels are only divided by a narrow Interbranch High. The Central Valley is slightly deeper than the East Branch. Collapse structures on both sidewalls of the Central Valley as well as on the western side of the East Branch indicate that these areas are unstable and hence prone to erosion. The channel fills, however, seem to be different. One strong reflector and almost no further penetration is observed in the thalweg of the Central Valley. In contrast, the East Branch is characterized by a broader band of dispersed high amplitude reflectors pointing to the aggradation of sand.

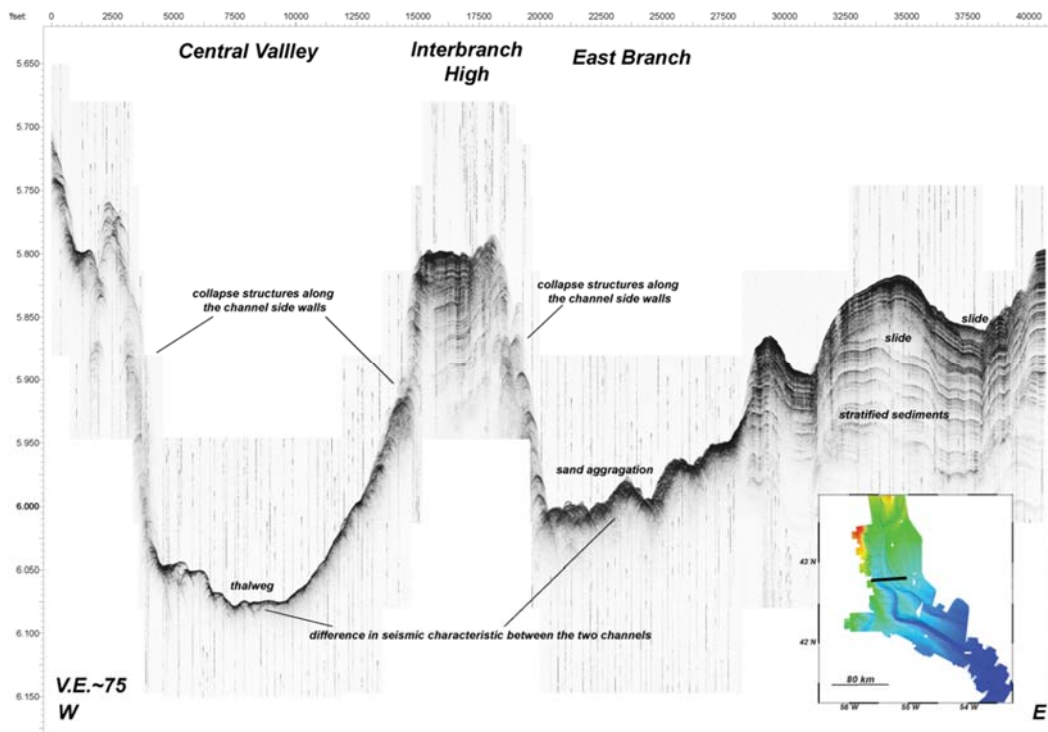


Fig. 5.6 PARASOUND profile crossing the Central Valley Channel at a location where the Interbranch High is narrow and hence the East Branch channel and the Central Valley are close together. See inset map for location of profile.

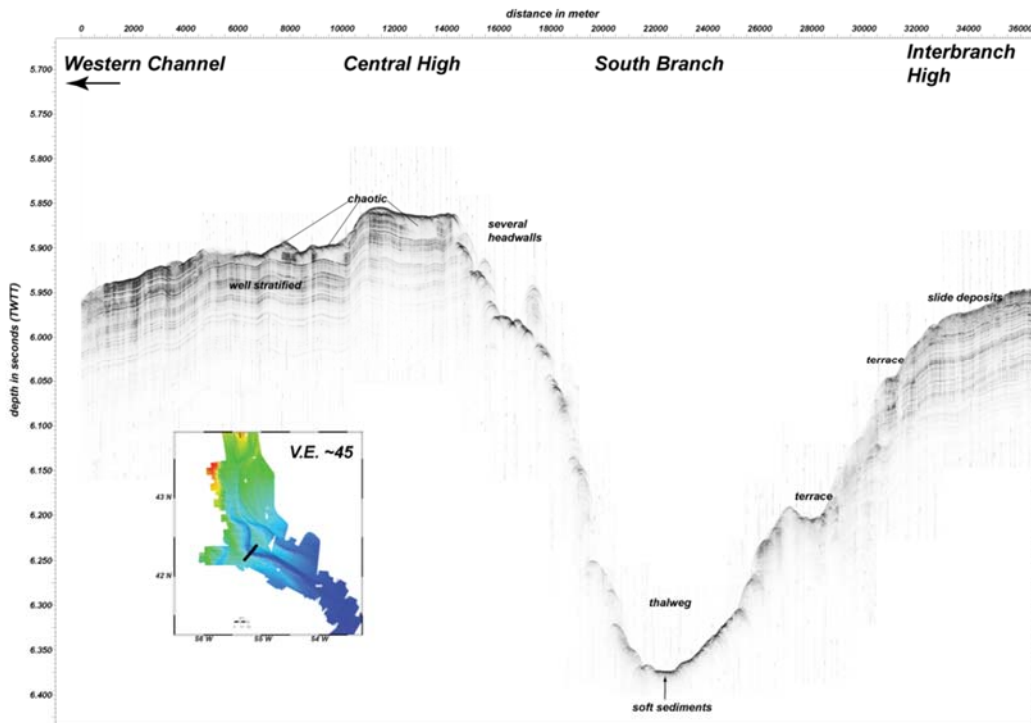


Fig. 5.7 PARASOUND profile collected across the South Branch at a location where the direction of the channel changes significantly. A giant box taken within the thalweg was completely filled with very soft sediments.

The Interbranch High seems to be an eroded remnant because well-stratified sediments are well imaged for major parts of the high. The Interbranch High is highly eroded and instable on each side (Fig. 5.6). An interlayering of slide deposits and well-stratified sediments is imaged east of the East branch. Such a pattern is characteristic for large areas of the southern working area.

Fig. 5.7 shows the South Branch where a distinctive change in direction from N-S to WSW-ENE occurs. Seismic characteristics of the Interbranch high are similar to those from the eastern Side of the East Branch (Figs 12 and 13), i.e. well stratified sediments in deeper parts overlain by chaotic units indicating recent sliding events (Fig. 5.7).

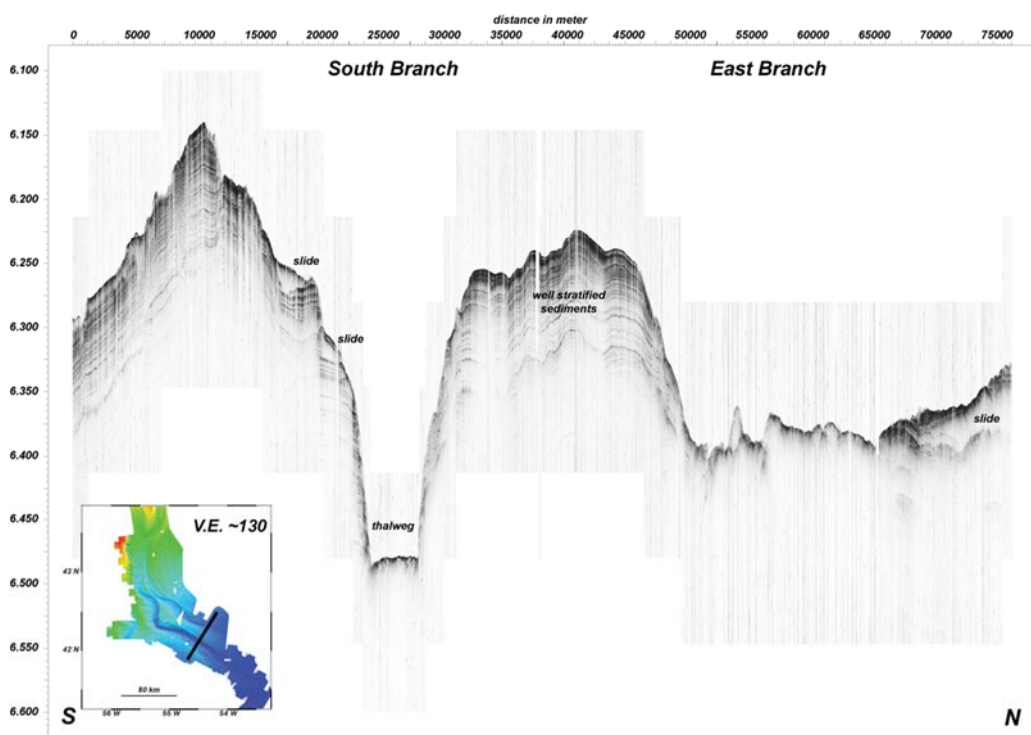


Fig. 5.8 PARASOUND profile the southern area of the channel system.

The Interbranch high is less eroded than further upslope. Along the southern channel wall, several scarps can be observed. The entire sidewall is eroded and instable. Some minor terraces with thin sediment deposits are found in the upper area of the southern side as well as along the northern side of the South Branch (Fig. 12). Such terraces were targeted during coring in order to reconstruct flow lines of turbidity currents. In the center of the thalweg, a small area characterized by a high-amplitude reflector with a smooth topography is visible (Fig. 5.7). Surprisingly, backscatter values are low for this section, and a box-corer taken at a similar location recovered very soft surface sediments. These soft sediments, however, are underlain by coarse sand in about 60 cm subsurface depth, which are probably imaged by the PARASOUND system (see chapter 5.3 - Sediment Sampling). The bathymetric map indicates an additional channel further to the west of the South Branch. In order to identify a coring station in this area, we crossed the Western Channel and collected hydroacoustic and seismic data. A prominent levee structure can be observed

on the western side of the channel (Fig. 5.9). East of the levee, the seafloor seems to be unstable and massive deposits of recent failure events can be found. The thalweg is imaged as high-amplitude reflector without significant sub-bottom penetration indicating a sandy canyon thalweg. However, a thin layer of soft sediments were sampled in the thalweg, which suggest a similar setting as for the South Branch (see above).

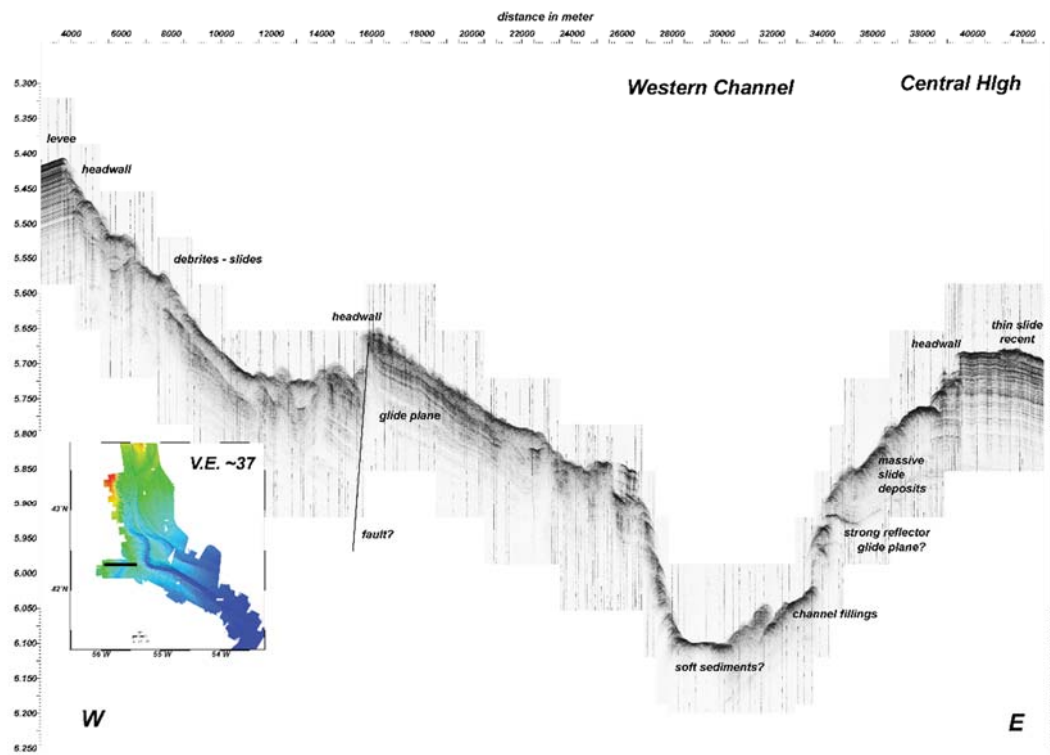


Fig. 5.9 PARASOUND profile crossing the western most channel. The sidewalls of the channel are characterized by several failures. Massive slide deposits can be found along the sidewalls.

Along the eastern side of the Western Channel, we imaged a massive (~20 m thick) transparent unit. A strong reflector below this unit indicates a possible glide plane (Fig. 5.9). Sediments further to the east are well stratified with the exception of a thin slide deposit at the surface (Fig. 5.9).

The area further south towards the deep basin is characterized by a deep and narrow South Branch channel but a shallow and wide East Branch (Fig. 5.8). Well-stratified sediments are present on the high separating the channels. On the southern side wall of the South Branch, two terraces with slide deposits are clearly visible. A ~30 m thick slide deposit marks the northern boundary of the East Branch. It is difficult to distinguish whether it still belongs to the active channel or if it is part of the sidewall. Towards the deep basin, the channels are less prominent as clearly observed on the bathymetric maps (Fig. 5.3).

5.1.3 ADCP

The Acoustic Doppler Current Profiler (ADCP) device is mounted to the vessel and provides an opportunity to measure the speed and direction of currents within the water column. It is an indirect measurement as it uses high frequency hydroacoustic sweeps (75 kHz Ocean Surveyor) to measure the speed and direction. A sound impulse will be reflected by very small and fine particles moving assumingly with the same speed as the water masses. The reflected signal is very low in energy because of the small size of the backscatter particles. If there is no motion in the water column the ADCP is not working properly. Caused by the particle movement, the receiving signal is frequency-shifted compared to the transmitted signal. The Doppler Effect characterizes the relative change in frequency between moving objects and hence calculates the speed and direction from the moving particles by analyzing the shift in frequency. Because the vessel is moving as well, the calculated water column speed is superimposed by the speed of the vessel and particle. Hence, processing of the data is needed including the incorporation of a navigation file into the data in order to distinguish the different movements. (Nortek As, 2008).

Depending on the ADCP settings, the transmitted beams can be separated in multiple horizontal sections by using the sound velocity profile. By knowing the signal travel distance in reference to the sound velocity profile, it matches different arrival times to certain depth or bin section. Each bin is considered by the ADCP to be an independent virtual transducer of the signal. The recorded time is averaged over 60 seconds within one bin in order to avoid system errors and to ensure that the data recording runs stable. A blanking distance of the ADCP caused by a cool down of the transducer after transmitting signals omits the recording of data with a very bad signal-to-noise ratio. The size and accuracy of these bin sections are mainly depending on the water depth and the blanking distance. Greater depth requires long-range transmission and therefore more energy and more time for recording and transmission. The accuracy decreases with greater depth, meaning the vertical size of the bin section increases. Greater bin section results in averaging the measured rather complex signal over a greater volume resulting in reduced accuracy. The size and the amount of the bin section can be set manually in the reference program taking the required depth into consideration (Nortek As, 2008).

On cruise MSM47 we performed the ADCP in Narrow Band mode with two different settings (i - 3000 m, ii - 5000 m) using the VmDas Software provided by Teledyne RD Instrument. (i) The first setting was adjusted for measurements up to a water depth of 3000 m. We set 128 bins with a single bin size of 24 m, a blanking distance of 12 m and a first time interval averaging time of 60 seconds. (ii) In water depth of about 5000 m, we used 128 bins with a single bin size of 40 m, a blanking distance of 20 m, and an averaging time of 60 seconds. During the entire MSM47 cruise, ADCP data were recorded parallel to the hydroacoustic and seismic surveys. There have been no check on the data quality so far.

5.2 High resolution 2D multichannel seismic profiling

(K. Lindhorst, C. Renkl, A. Bräunig, I. Mücke, L. Wiesenber, S. Mader, I. Schulten, M. Merl, M. Vallee)

A Geometrics GeoEel streamer consisting of solid state and oil filled sections and two standard 1,71 GI-guns were used to acquire high-resolution multichannel seismic data. The aim was to resolve small-scale sedimentary structures and closely spaced layers on a meter scale, which can usually not be resolved by means of conventional seismic systems. Figure 015 gives an outline of the system setups as it were used during MSM47. Table 5.1 lists the individual setting for each profile. A list of seismic profiles is given in Table 7.4.

Fig. 5.10 Deck and seismic gun setting during Cruise MSM47.

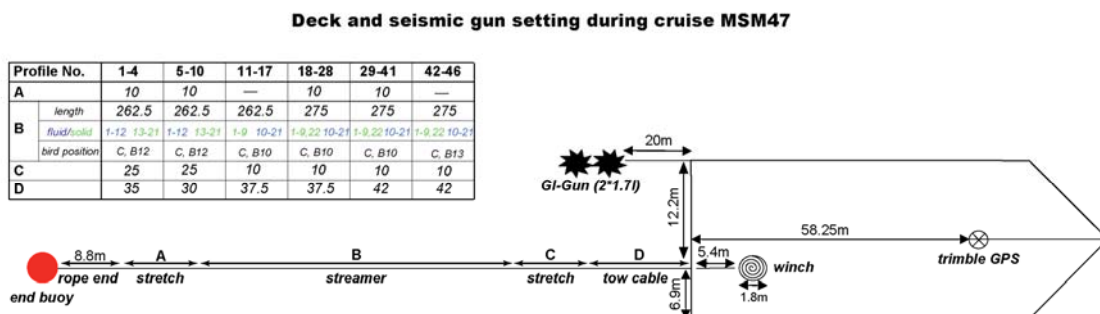


Table 5.1: Source and receiver settings for all seismic profiles.

Profile	Source, mode, shooting rate (s)	Streamer	Birds
P100 SOL001- EOL003	2*1.7l GI-Gun, harmonic mode, shot rate 7s, record length 6.5s	168 channels, 1*25m-stretch (behind the tow cable), 1*10m stretch (at the end of the streamer) Twelve 12.5m fluid filled sections (section 1-12), Nine 12.5m solid state sections (section 13-21)	Start first stretch, Start section 12
P200 SOL004- EOL006	2*1.7l GI-Gun, harmonic mode, shot rate 7s, record length 6.5s	168 channels, 1*25m-stretch (behind the tow cable), 1*10m stretch (at the end of the streamer) Twelve 12.5m fluid filled sections (section 1-12), Nine 12.5m solid state sections (section 13-21)	Start first stretch, Start section 12
P300 SOL006- EOL010	2*1.7l GI-Gun, harmonic mode, shot rate 6s, record length 5.5s	168 channels, 1*25m-stretch (behind the tow cable), 1*10m stretch (at the end of the streamer) Twelve 12.5m fluid filled sections (section 1-12), Nine 12.5m solid state sections (section 13-21)	Start first stretch, Start section 12
P400 SOL011- EOL017	2*1.7l GI-Gun, harmonic mode, shot rate 6s, record length 5.5s	168 channels, 1*10m-stretch (behind the tow cable), Nine 12.5m solid state sections (section 1-9), Twelve 12.5m fluid filled sections (section 10-21)	Stretch section, Start section 13
P500 SOL018- EOL023	2*1.7l GI-Gun, harmonic mode, shot rate 6s, record length 5.5s	176 channels, 1*10m-stretch (behind the tow cable), 1*10m stretch (at the end of the streamer), Ten 12.5m solid state sections (section 1-9, 22), Twelve 12.5m fluid filled sections (section 10-21)	Stretch section, Start section 13
P600 SOL024- EOL028	2*1.7l GI-Gun, harmonic mode, shot rate 5-8s, record length 3.5s, delay 0- 4s	176 channels, 1*10m-stretch (behind the tow cable), 1*10m stretch (at the end of the streamer), Ten 12.5m solid state sections (section 1-9, 22), Twelve 12.5m fluid filled sections (section 10-21)	Stretch section, Start section 13

Profile	Source, mode, shooting rate (s)	Streamer	Birds
P700 SOL029- EOL035	2*1.7l GI-Gun, harmonic mode, shot rate 8.5s, record length 3.5s, delay 5s	176 channels, 1*10m-stretch (behind the tow cable), 1*10m stretch (at the end of the streamer), Ten 12.5m solid state sections (section 1-9, 22), Twelve 12.5m fluid filled sections (section 10-21)	Stretch section, Start section 13
P800 SOL036- EOL038	2*1.7l GI-Gun, harmonic mode, shot rate 7.5-8.5s, record length 3.5s, delay 4-5s	176 channels, 1*10m-stretch (behind the tow cable), 1*10m stretch (at the end of the streamer), Ten 12.5m solid state sections (section 1-9, 22), Twelve 12.5m fluid filled sections (section 10-21)	Stretch section, Start section 13
P900 SOL039- EOL041	2*1.7l GI-Gun, harmonic mode, shot rate 7.5-8.5s, record length 3.5s, delay 4-5s	176 channels, 1*10m-stretch (behind the tow cable), 1*10m stretch (at the end of the streamer), Ten 12.5m solid state sections (section 1-9, 22), Twelve 12.5m fluid filled sections (section 10-21)	Stretch section, Start section 13
P1000 SOL042- EOL045	2*1.7l GI-Gun, harmonic mode, shot rate 8.5s, record length 3.5s, delay 5s	176 channels, 1*10m-stretch (behind the tow cable), Ten 12.5m solid state sections (section 1-9, 22), Twelve 12.5m fluid filled sections (section 10-21)	Stretch section, Start section 13
P1100 L046	2*1.7l GI-Gun, harmonic mode, shot rate 8.5s, record length 3.5s, delay 5s	176 channels, 1*10m-stretch (behind the tow cable), Ten 12.5m solid state sections (section 1-9, 22), Twelve 12.5m fluid filled sections (section 10-21)	Stretch section, Start section 13

5.2.1 System components

Seismic sources and trigger

During seismic surveying, two standard GI-Guns were used as source; both of them were shot in a harmonic mode (2 * 1.7 l). The GI-Guns were connected in line to one gun-hanger 205 cm apart, each GI-Gun hanging on two chains 50 cm beneath. The GI-Guns were deployed with the port side crane and towed ~20 m behind the ship's stern (Fig. 5.10). Each gun had an elongated buoy connected to the gun-hanger by two rope loops, which stabilized the guns in a horizontal position and kept them in ~2 m depth. The Injector of the GI guns were triggered with a delay of 42 ms with respect to the Generator signal, which basically eliminated the bubble signal. Guns were shot between 150 to 163 bar. Shooting intervals varied between 6 s and 8.5 s (depending on water depth) resulting in a shot point distance between ~15 m and ~20 m at 4.5 knots. The guns worked reliable during the cruise with one exception as one of the firing lines broke and had to be replaced. A Long Shot unit was used as gun controller. The arming point for the gun was set to 60 ms. A trigger was generated by a custom-made unit allowing to adjust shooting rates and delay times based on the water depth.

Streamer-system

A digital streamer (Geometrics GeoEel) was used for receiving the seismic signals. The system consists of a tow cable (~80 m, with variable length in the water, see Fig. 5.10), one vibration isolation section each (10 m long) at the beginning and end of the active part of the streamer, and up to 22 active sections (each 12.5 m long). An active section contains

eight channels (channel spacing of 1.56 m, total length of 12.5 m) resulting in 176 channels for the entire streamer (Fig. 5.10). The streamer was operated in different configurations. A detailed description of the streamer configuration is given in Table 5.1. One A/D converter module belongs to each active section. These A/D converter modules are small Linux computers. Communication between the A/D converter modules and the recording system in the lab is via TCP/IP. A repeater was located between the deck cable and the tow cable (Lead-In). The SPSU manages the power supply and communication between the recording system and the A/D converter modules. The recording system is described below. Additionally, two birds were attached to the streamer (see below). Designated streamer depth was 3 m. A large orange buoy with reflector tape was attached to the tail swivel.

Bird Controller

Two Oyo Geospace Bird Remote Units (RUs) were deployed at the streamer. The locations of the birds are listed in Table 5.1. Both RUs have adjustable wings. A bird controller in the seismic lab controls the RUs. Controller and RUs communicate via communication coils nested within the streamer. A twisted pair wire within the deck cable connects controller and coils. Designated streamer depth was three meters. The RUs thus forced the streamer to the chosen depth by adjusting the wing angles accordingly. The communication with the birds were reliable during the first five surveys until Bird 1 lost communication. However, the wings of the bird were still in the right angle to ensure that the desired depth of 3 m was still valid. During the last profile, we also lost communication to the second Bird. However, a close inspection of the data showed that the birds worked reliable and kept the streamer at the designated depth.

Data acquisition systems

Data were recorded using an acquisition software provided by Geometrics. The analogue signal was digitized with 2 kHz. The data was recorded as multiplexed SEG-D files. One file was generated per shot. The acquisition PC allowed online quality control by displaying shot gathers, a noise window, and the frequency spectrum for each shot. The cycle time of shots is displayed as well. The software also allows online NMO-Correction and stacking of data for selectable stacked sections. Several log-files record parameters such as shot time and position. A first processing step included the conversion of SEG-D into SEG-Y files and a setup of the delay value in the header of the SEG-Y files.

5.2.2 First results of seismic survey

Preliminary data processing was carried out for all profiles onboard. Six channels (usually channels 10-15) of each shot were filtered (30/60/600/1000) and stacked vertically. The brute stacks were loaded to a seismic interpretation software (IHS Kingdom Suite 8.8) and used for preliminary interpretation. In total, we collected about 1500 km of seismic profiles. Data quality is general very good but some profiles were collected at very rough sea states decreasing the signal-to-noise ratio significantly. Due to the large number of channels, final processing will provide excellent images. We collected seismic data in two areas: (1) the

northern area where a good bathymetric map as well as seismic lines were already available and (2) in the southern area, which was not surveyed in detail before.

Northern Area

A seismic cross section imaging the internal structure of the St. Pierre Slope is shown in Fig. 016. The most prominent feature is a probable fault structure at the upper slope.

A headwall marks the surface expression of the potential fault. The fault seems to mark the boundary between well-stratified more or less undisturbed sediments upslope of the headwall and several slide deposits and minor scarps downslope of the headwall (Fig. 5.11). It is likely that this fault has been recently active and induced a major sliding event along the St. Pierre Slope.

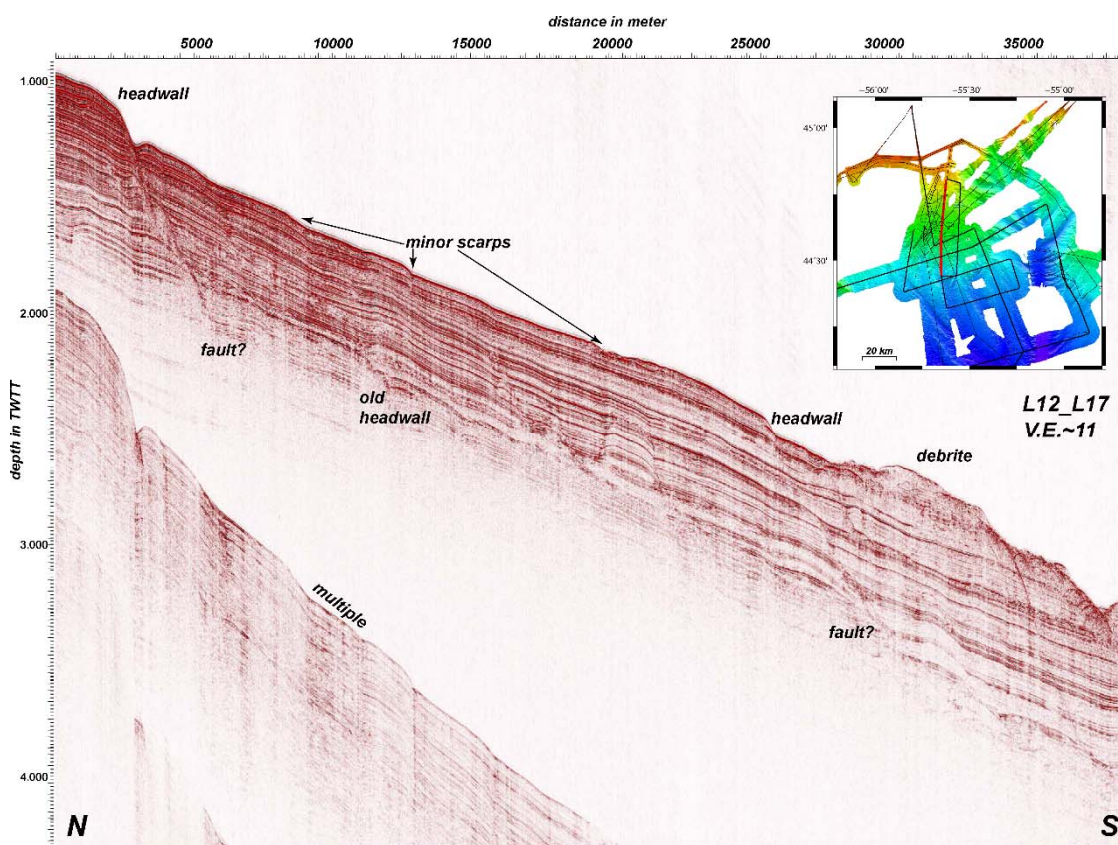


Fig. 5.11 Combined seismic cross sections 12 and 17 imaging the internal structure of the St. Pierre Slope Area. See inset map for location of profile.

Potential faults are imaged on several profiles in this area. A detailed analysis of all available data (newly collected and previously available data) is needed to check, whether this fault contributed to the 1929 Grand Banks event (landslide and tsunami). A major debrite at the surface has been identified further downslope. Several additional smaller headwalls or minor scarps suggest that the sediments along the St. Pierre slope have been unstable in the past and are prone to failure.

Southern Area

Several seismic lines were collected in the Southern Area in order to investigate the architecture of the complex channel system, which was the main pathway for the turbidity currents during the 1929 event. At around 43.5 °N, the Grand Banks Channel merge with the main Laurentian Channel System. Seismic Profile 42 is collected just beneath the merging point. It mainly images the internal structure of the Laurantian Fan east of the channel system (Fig. 5.12). The channel thalweg is characterized by high-amplitude reflectors of moderate continuity suggesting an aggradation of sandy sediments. An older boundary of the channel is marked by a dashed line.

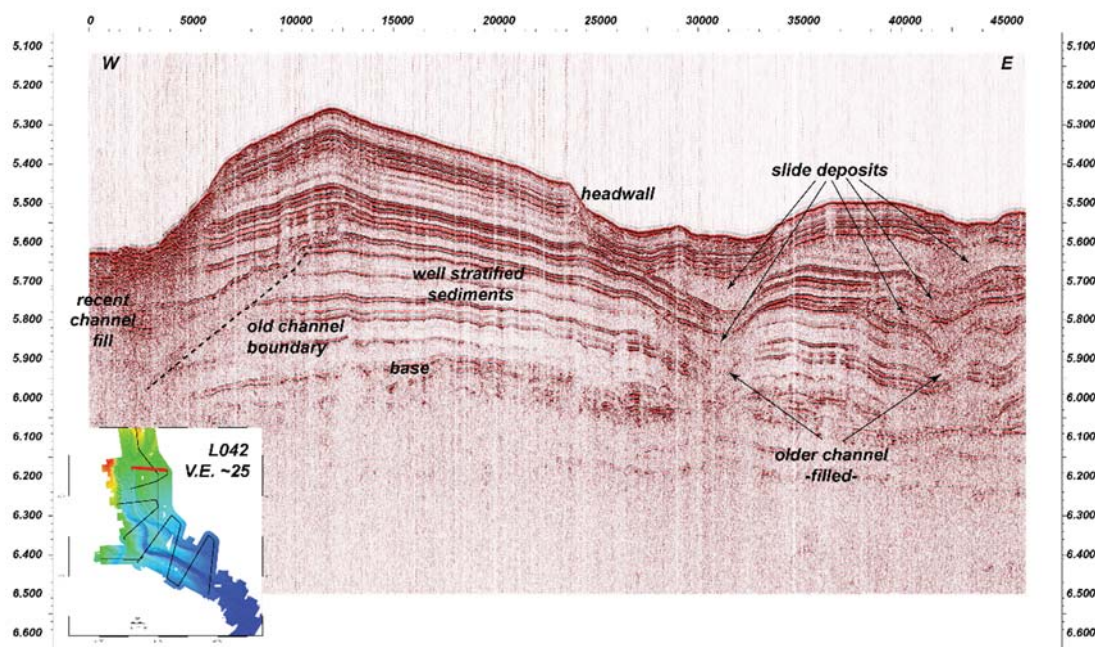


Fig. 5.12 Seismic cross section 042 imaging the channel system just south of the merging point of the Grand Banks Channel the Laurentian Channel System. See inset map for location of profile.

The sediments east of the channel show a levee-like structure with well-stratified sediments. Some major transparent units indicate slide deposits. Slide deposits are more abundant in the eastern part of the profile at a greater distance to the channel. Some buried filled channels are found as well. A diffuse reflector that can be traced throughout the profile seems to mark the base of the channel system as it is not cut the by the channel. Full processing of the data will allow to image structures beneath this diffuse reflector more clearly.

Profile 29 is located further downslope and allows a comparison of the East and South Branch (Fig. 5.13). In general, the East Branch is shallower and seems to be partly filled by sandy deposits, whereas the South Branch is quite deep and not showing any significant sedimentary fill. However, chaotic high-amplitude reflectors extend from the thalweg in a northeasterly direction and downwards. This unit may represent sandy sediments deposited at the former thalweg. Hence, the east branch would mainly be characterized by an

aggrading channel floor while the South Branch shows lateral migration and aggradation. The absence of stratified deposits in either of the channel branches suggests that both branches have been active in the younger past. Several erosional structures are especially found at the walls of the South Branch supporting recent channel activity leading to base erosion and subsequent failures of the canyon walls. A thick (~50 m) slide can be found along the northern side of the South Branch.

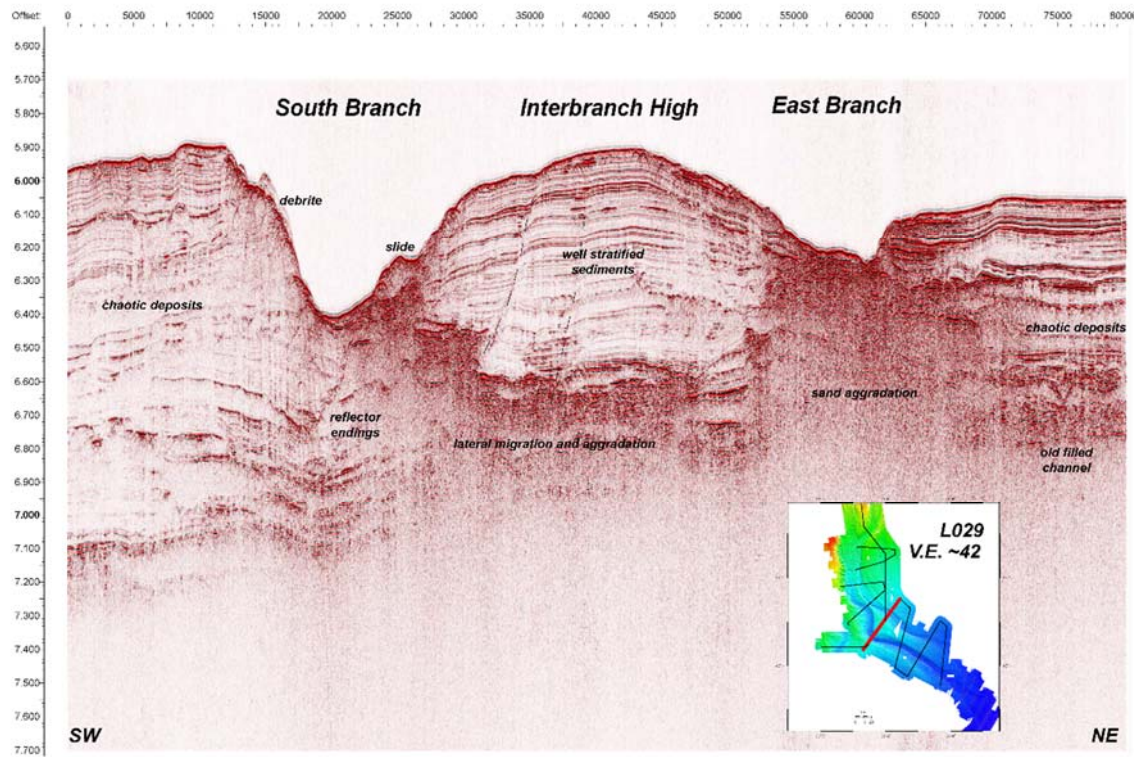


Fig. 5.13 Seismic cross section 029 crossing the South and East Branch and imaging the internal structure of the Interbranch High. Dashed lines indicate possible fault structures or fluid pathways which will be analyzed in detailed after final processing.

The Interbranch High is characterized by well-stratified sediments (Fig. 5.13). Two minor faults are visible (dashed lines on Fig. 5.13). They seem to form pathways for fluids as indicated by spots of high amplitude reflectors within the upper sediments. The most recent sediments on top of the Interbranch High also include some mass transport deposits as indicated by several hyperbolas at or very close the sea floor. The internal structure of the Interbranch High is significantly different compared to the sedimentary structure southwest and northeast of the channel system, which is characterized by an interlayering of well stratified and chaotic to transparent units. The chaotic units represent mass transport deposits. The absence of the chaotic to transparent units at the Interbranch High suggest that most landslides did not reach the Interbranch High as it is protected by the channel system.

A cross-section of the Western Channel is shown in Fig. 5.14. The existence of this channel was already documented during previous expeditions. A prominent right-handed

levee structure marks the western side of the channel. Both sidewalls are heavily eroded and experienced several mass failure events.

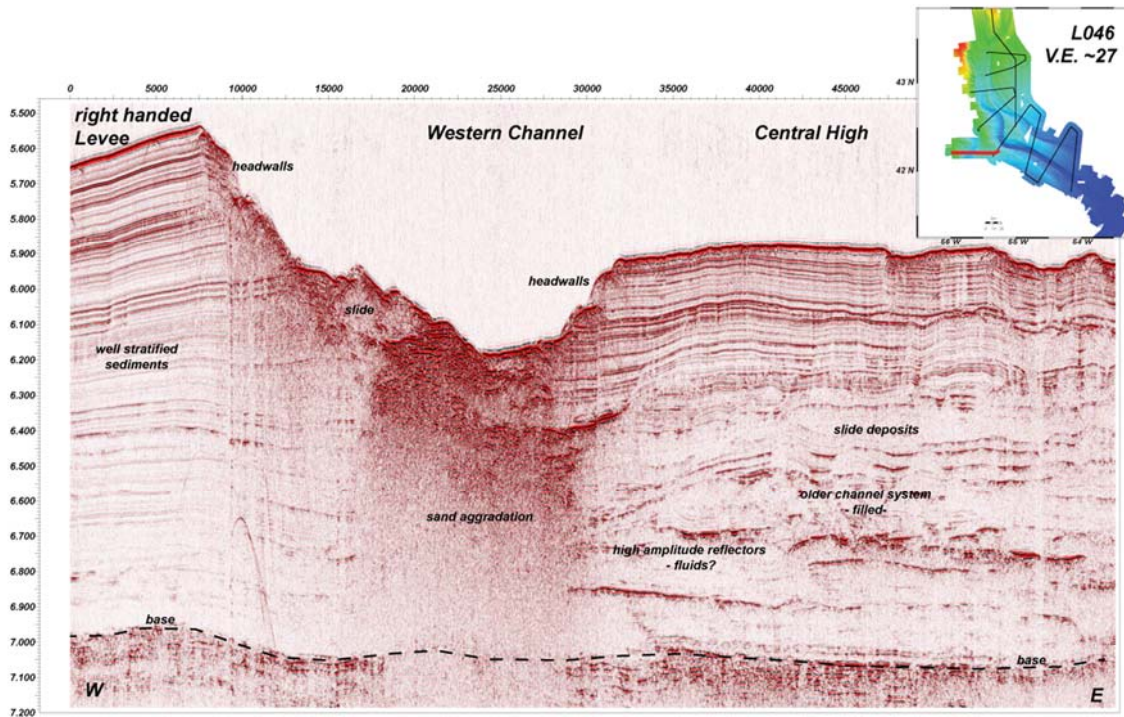


Fig. 5.14 Seismic section 046 crossing the Western Channel. See inset map for location of profile.

A massive slide deposit (>50 m thick) is imaged in the western part of the channel. The channel itself seems to be filled by sand and shows an aggradational pattern. The area east of the Western Channel is called Central High. The upper part of this high is dominated by well-stratified sediments but several chaotic to transparent units are clearly visible further down. Several slides are stacked on top of each. A diffuse reflector characterized by relatively high amplitudes (dashed line) marks the base of the Western Channel System (Fig. 5.14).

5.3 Sediment Sampling

(A. Georgioupolou, P. Feldens, C. Stevenson, J. Llopis, L. Mehringer, J.-P. Schwarz, M. Schönke, B. Wegener)

During cruise MSM47, cores were mainly taken in order to find the deposit of the 1929 slope failure. The St Pierre slope in the northern study area and the lower Laurentian Channel in the southern area were targeted as cable breaks have been documented there, which means the flow must have come through there. We used a standard Gravity Corer (GC) and a Giant Box Corer (GBC) at selected stations. A station list is given in Table 7.3. The core locations are shown together with seismic lines on Fig. 5.3.

The 1929 event is very young in geological terms and with only 86 years since its occurrence; we were expecting to find it at the seafloor, without a hemipelagic cover on it which would take a few hundred to even thousands of years to deposit. The GBC was used in areas, where we expected coarse-grained surface covers and when we wanted to ensure

that the GC was sampling the surface sediments. The GBC was applied at 15 stations and the GC at 30 stations (Table 7.3), several times, they were both used at the same station. The top weight of the GC is 2 tons, and 25 times out of the 30 stations it retrieved sediments successfully. The GC was used with station-individual lengths of 3, 5, 8, 10 or 15 m (Table 7.3). Total core recovery was about 130 m.

5.3.1 Core processing

Gravity corer

After retrieval, the core liners were cut into one-meter sections and closed with caps. They were then split lengthways and each half of the core section was labeled including core depth (starting at the top of the core), MSM-47, ongoing geology station number and designation for archive (A) and working (W) half. Generally, the top of each core section has a yellow cap, while the base has a white cap. The halves were stored in D-Tubes following onboard processing. Few cores were not split; two of them are to be used for further geotechnical analysis in the laboratory and two of them contained very fluid deposits and it was decided to cap them and take them back to the lab for further processing (CT scan, etc). Sub-samples for grain size analysis were taken from the working half every 5 -10 cm, with extra samples as indicated by layers and texture.

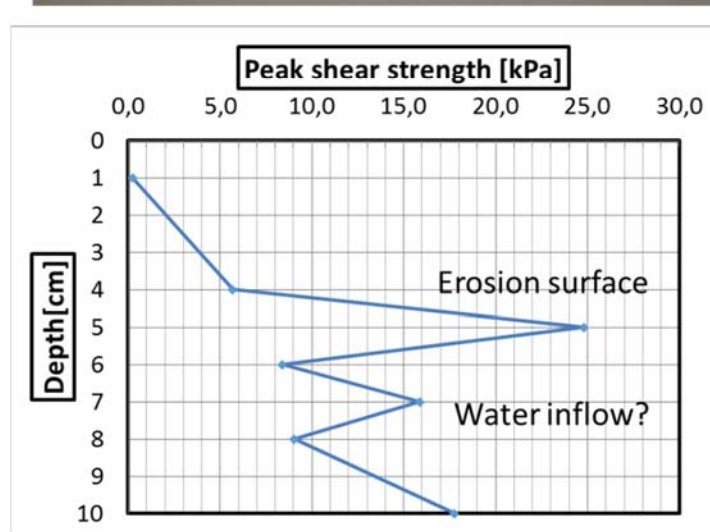
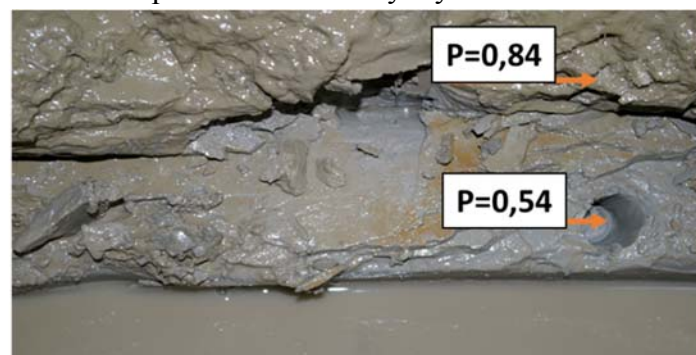


Fig. 5.15 Display of undrained shear strength values measured by fall cones through a box corer profile. The uppermost mud is extremely weak with high porosity (P), which decreases dramatically at an erosional boundary in 4-5 cm depth

Two to three fall cone tests were done every 5 to 10 cm to determine the undrained shear strength on most core sections. Extra tests were achieved as determined by layering and texture. For selected cores, test of undrained shear strength using a shear vane were done. For every processed core section, 3 to 7 samples of 2 ml to 7 ml in volume were taken for porosity tests, again according to layering and texture. The porosity samples are stored in water-tight Nunc-sampling tubes. Their weight was measured directly on board using a stabilized scale. In addition to the electronic stabilization, 300 to 1000 individual measurements were averaged for every sample to reduce impact of ship movements on the result. Following the determination of wet weight, samples were dried at 80° for 48 to 72 hours. Subsequently, the dry weight was measured using the same procedure. The archive halves were photographed, described in detail and thin slides for the x-radiograph negatives were retrieved.

Box corer

Following retrieval of the box corer, two push cores were taken and labeled according to their geological station number. Porosity samples were taken as soon as the box corer was opened. Where possible, a clean surface was created to retrieve material for the creation of x-radiograph negatives. Due to the unavoidable compression of subsamples during retrieval, for most box corers, shear strength measurements were done within the box corer (Fig. 5.15). Following the surface measurements of undrained shear strength, 1 cm to 2 cm of sediment were carefully removed using a spatula, and the measurements were repeated. Using this method, undrained shear strength could be measured until approx. 10 cm to 15 cm depth.

5.3.2 Preliminary coring results

Gravity and box coring were focused in four main areas, (1) the Grand Banks Valley, (2) the St Pierre slope in the northern working area, (3) the confluence of the Grand Banks Valley with the Eastern Valley, and (4) the lower Eastern and Western Valleys in the southern working area (Figs 05 and 08).

Northern Working Area

Grand Banks Valley

Three areas were targeted at the Grand Banks Valley (Fig. 5.3). One core was taken on the eastern margin of the Grand Banks Valley (MSM47-001), approximately 500 m above the canyon thalweg (WD=2436 m). The backscatter here appeared soft and the PARASOUND profile showed good penetration. The 6 m set up was chosen (MSM47-001-2) but it over-penetrated and buried itself all the way to the rope. It was decided to try again in the same place with a 14 m set up and retrieved 8.1 m. This core sampled a series of muddy turbidites with reddish colour, alternating with greenish-grey background mud. The turbidites had characteristic sharp colour changes at the base.

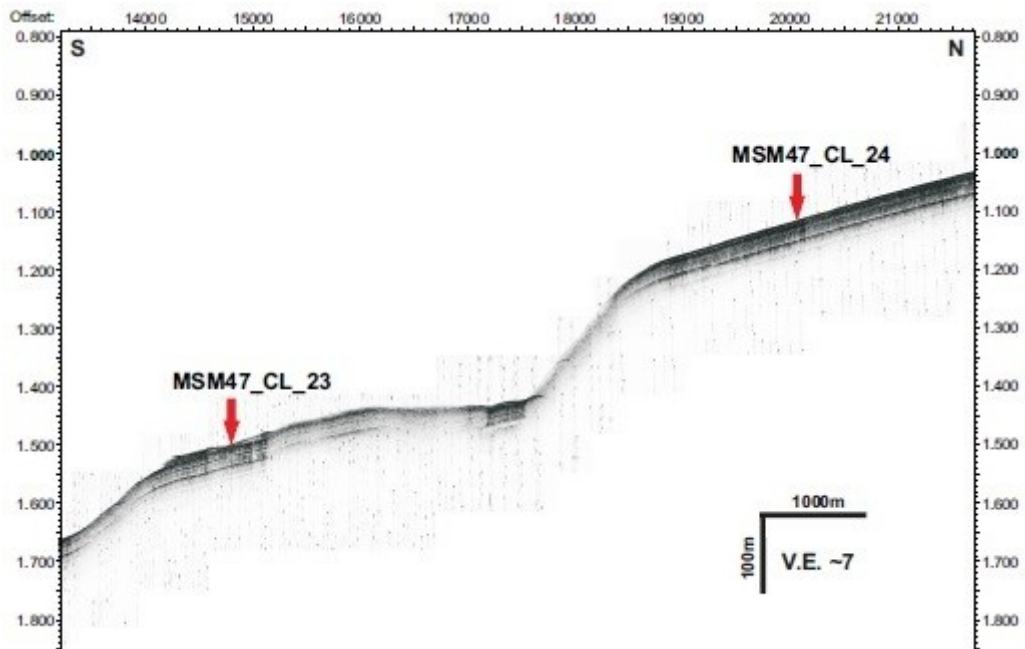


Fig. 5.16 PARASOUND profile crossing the scarp on the upper St Pierre slope. Gravity cores MSM47-23 and 24 were taken along this profile. Location of profile is shown in Fig. 5.4

MSM47-7-1 Gravity core from chaotic unit covering the St Pierre slope (topographic high):
Soft drape, then debrite (indicated with orange) overlying hemipelagic with H1 towards
base - correlates with MSM47-6-2

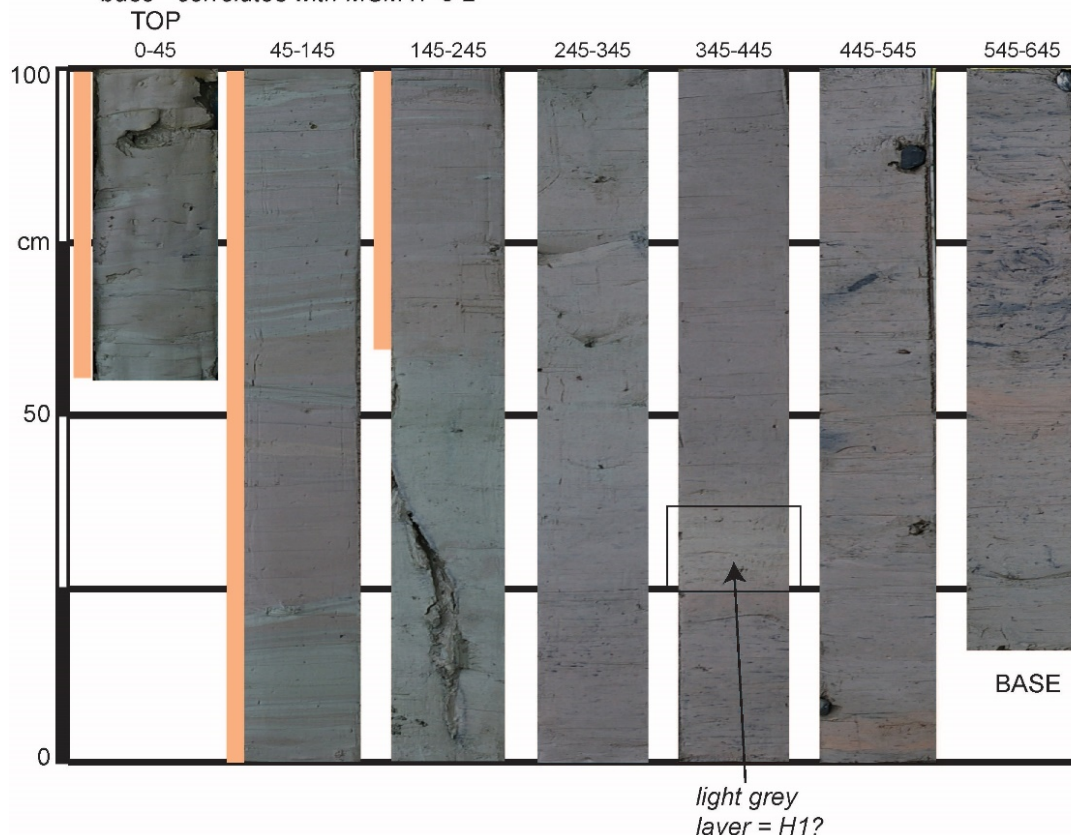


Fig. 5.17 Photograph of Gravity Core MSM47-7-1. See Fig. 5.3 for location of core.

Two locations were chosen closer to the thalweg, one at 30 m (MSM47-002-1) and one at 80 m (MSM47-003-1) elevation, both with good sub-seafloor penetration on the PARASOUND. MSM47-002-1 was a box corer and did not penetrate too deeply, but was stopped by a stiff, highly compacted, mud layer, which must be an erosional surface. The box corer at MSM47-003-1 again sampled an erosional surface of compact clay. The gravity corer was deployed at 3 m set up (MSM47-003-2) and retrieved 2.56 m of stiff laminated mud.

St Pierre Slope

The St Pierre slope is where the epicentre of the 1929 earthquake most likely was and it has been suggested that slope instability initiated here. Eight coring locations were selected here, most of them were targeted both with the gravity corer and the box corer, and two of the gravity cores were sealed for geotechnics (MSM47-004-3 and 024-1).

The St Pierre slope is dissected by multiple scarps, none of which looks fresh (Fig. 5.16). We took cores below and above scarps to assess whether any of them had been recently reactivated. We started at the bottom of the slope with MSM47-004-1, which bent but retrieved 3.95 m and we found a young muddy debrite at the top of the core. The debrite is very soft in the top 45 cm and continues downcore into sheared pink, mint-green and grey mud laminae. We kept sampling upslope until we reached a location upslope of a scarp that did not contain the debrite. Cores 005, 006, 007 (Fig. 5.18), and 026 do contain the debrite in thicknesses of about 2 m, whereas 023 and 10 do not.

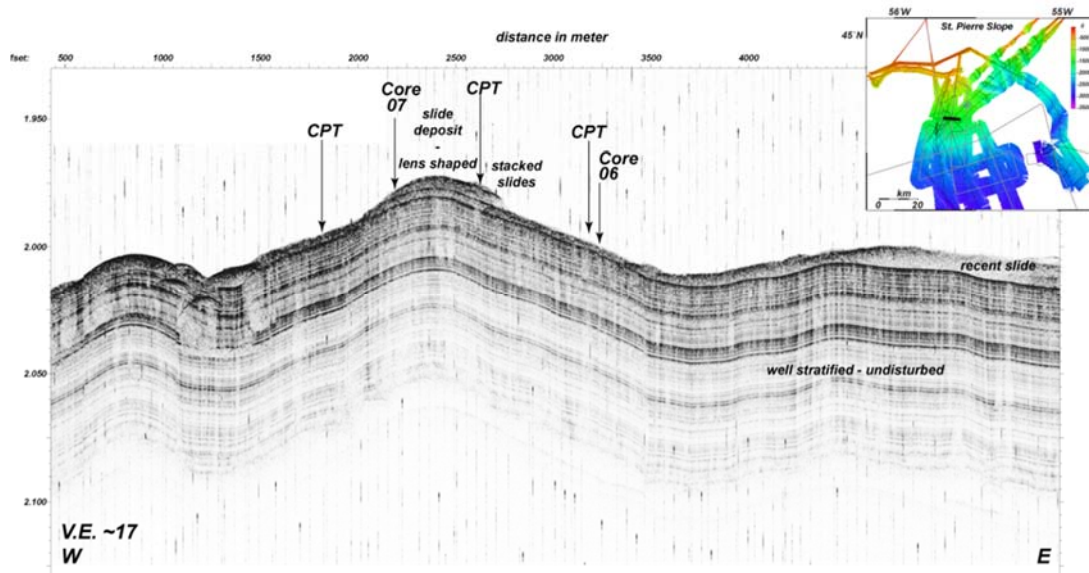


Fig. 5.18 PARASOUND profile on the middle St Pierre slope across gravity core MSM47-6-2 and 7-1. Location of profile is shown in Fig. 5.3.

At the top of GC 010-2 we found a 60 cm layer of very soft silty mud with a mousse-like texture and below it sandy turbidites and hemipelagites with lithologies that are found sheared in the young debrite downslope, so we conclude that the debrite originates from a reactivation of the long scarp on the Upper St Pierre slope. The fact that Core 023-1 does not contain the debrite probably means that the scarp was either partially reactivated on its

northeastern edge or if the entire scarp was reactivated, location 023 was bypassed. There is a prominent light grey stiff mud layer in all the cores, which helps us correlate them and estimate the depth of erosion of the debrite. This layer also correlates with the prominent PARASOUND reflector at the base of the acoustic character of the debrite (Fig. 5.18). One box core and one gravity core (012-1 and 012-2, respectively) were taken from the upper Laurentian Channel in the Eastern Valley near the shelf edge. The GC was used with the 5 m set up and the entire liner was filled (100% retrieval). It may have over-penetrated a bit but there does not appear to be a young debrite present, only one 2 m downcore. We therefore believe that the shelf edge did not fail in 1929 and therefore is not responsible for the generation of the catastrophic landslides.

Southern Working area

Confluence of Eastern Valley with Grand Banks Valley

Two core locations were chosen at the confluence of the Grand Banks Valley and the Eastern Valley in an attempt to assess the run up height of the flows that flowed down the Grand Banks Valley. We first tried at location 027 with GC (027-1), which bounced but sand had smeared on the side of the barrel and so we tried again with the box corer (027-2), which came back full of sand. We then targeted the pinch out of the sand with the GC a bit further upslope (028-1). MSM47-028-1 retrieved 4.89m (Fig. 5.19). At the top, we found 30 cm of gravelly sand, which we believe, is the deposit of the 1929 event, in an erosional contact with smooth red clayey mud at the bottom of the core, itself interrupted by three intervals of grey, black-stained mud.

MSM47-28-1 Gravity core from confluence of Grand Banks and Eastern Valley, 100m up from thalweg, outer bend: VCS bed with ragged mud cap, erosive contact to red mud

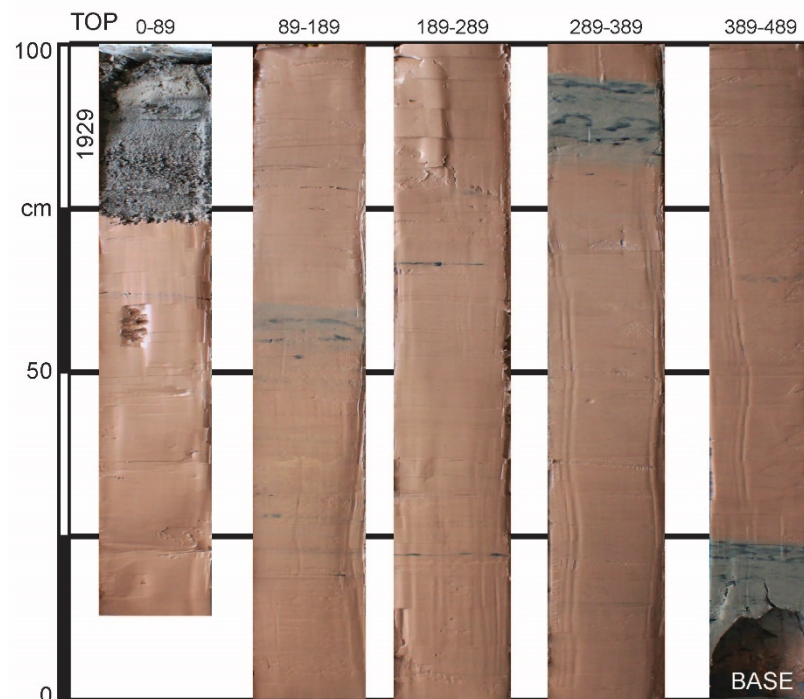


Fig. 5.19 Photograph of Gravity Core MSM47-28-1. See Fig. 5.3 for location of core.

Lower Eastern and Western Valleys

Five core transects were performed in the lower slope area; where the Eastern Valley is split into a Southern and an Eastern Branch, separated by an Interbranch High. Transect 1 crosses the Eastern Branch, transect 2 crosses the Southern Branch, transects 3 and 4 cross the Southern Branch further downslope, and transect 5 crosses the Western Channel. The aim was to establish whether the 1929 flow utilized all three channels towards the Sohm Abyssal Plain and to assess how thick the flow was by determining the trim line.

MSM47-21-1 Gravity core from inner bend terrace of Southern Channel 187m up from thalweg:
Soupy graded turbidite sand to sandy mud, overlying red and grey slide deposits

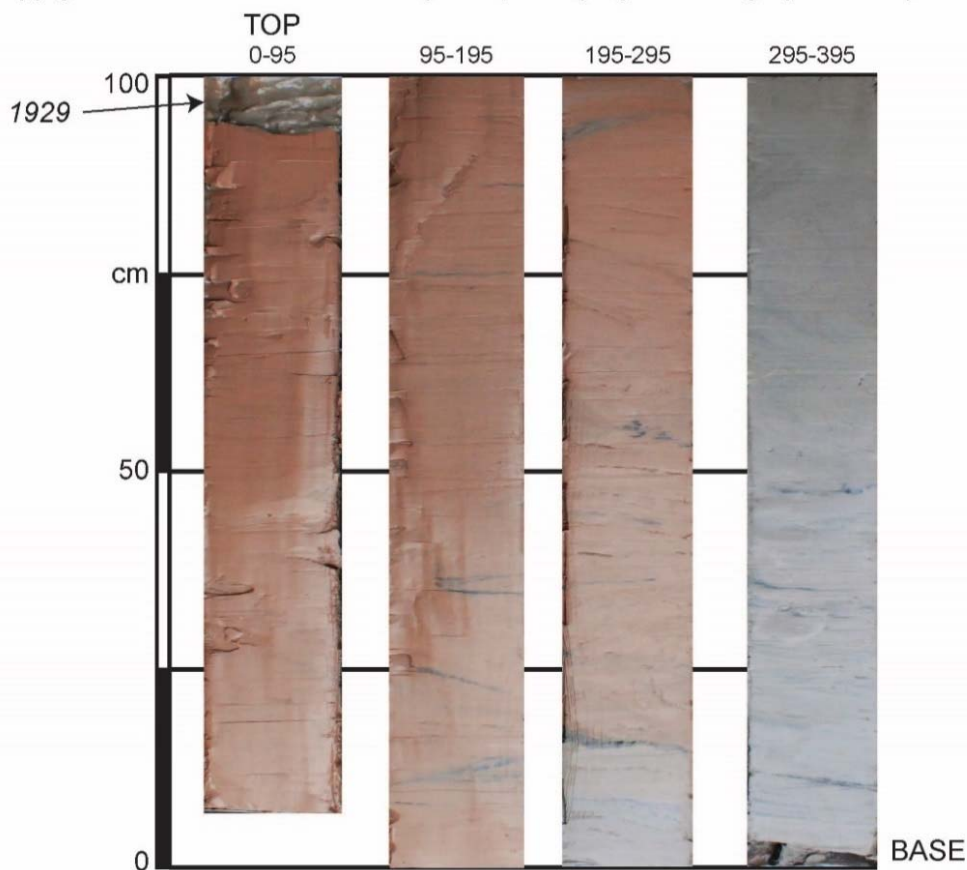


Fig. 5.20 Photograph of Gravity Core MSM47-21-1. See Fig. 5.3 for location of core.

Transect 1

Transect 1 is north-south orientated and made up of four stations. Stations 016 (south) and 018 (north) are flanking the core transect and are taken from the higher slope, and 017 and 019 are taken from terraces 150 and 175m respectively above the thalweg. Station 016-2 had a retrieval of 5.97m and appears undisturbed by the 1929 event, so it gives us a good understanding of the background sedimentary sequence. Core 017-1 bounced, and 018-1 and 019-1 both had a 1cm smear of sandy mud draping the Holocene hemipelagite, i.e. the 1929 turbidite deposited here but was not erosive and therefore draped the background sediments. No sand associated with 1929 was retrieved from the East Branch.

Transect 2

Transect 2 links with transect 1 at location 016. It goes across the inner and the outer bend of the South Branch (Fig. 5.3). MSM47-021, 022 and 029 target terraces on the left-channel margin (inner bend), 013, 030 and 032 terraces on the right-channel margin (outer) and 031 the channel thalweg. The left margin was expected to be more depositional as it is on the inner bend. However, only GC MSM47-021-1 at an elevation of 125 m above the thalweg contained a thicker turbidite mud (~10 cm) directly on top of the red muds (Fig. 5.20).

The lower terraces (022 and 029) are covered with gravel and sand and both GC and GBC failed to retrieve more than a few grains (bagged). On the other side of the margin, on the outer bend that is expected to be affected by the more energetic part of the flow, turbidite mud is found on three different elevations above the channel thalweg (>300m – GC 013-1; 210m – GC 030-1; 100m – GBC 032-1). An example of a peak strength and porosity measurement can be seen on figure Fig. 5.22.

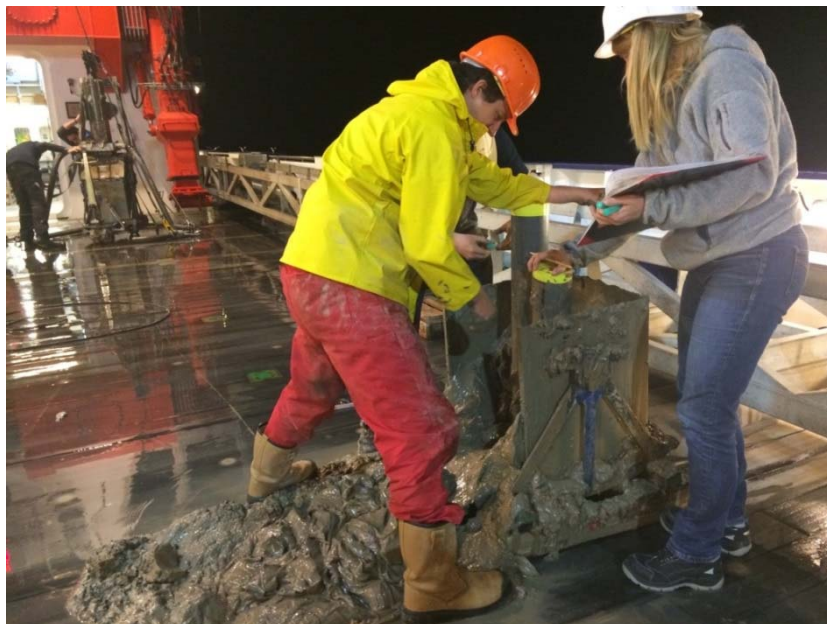


Fig. 5.21 Photograph of Box Core MSM47-31-1. Note the very fluid mud. Two push cores were retrieved but were not opened onboard. See Fig. 5.3 for location of core.

However, 100 m above the thalweg we also find turbidite sand underneath the turbidite mud, resting on compacted mud, which we interpret as an erosional surface. The backscatter signature in the channel thalweg indicated that, counter-intuitively, the seafloor was soft. The PARASOUND signature did not entirely agree. The box corer and the gravity corer were deployed in this location and 031-1 (GBC, Fig. 5.21) retrieved 70 cm of very soft, very fluid turbidite mud on top of sand.

Transect 3

Two cores constitute this transect, 014 and 015. Further downslope of 031, in the thalweg at site 014, the GC was deployed but it bounced. Sand silt and fine sand were smeared on the barrel. Station 015, taken on the Interbranch High downslope from 016, is very similar to 016, and is draped by 1 cm of the 1929 turbidite mud.

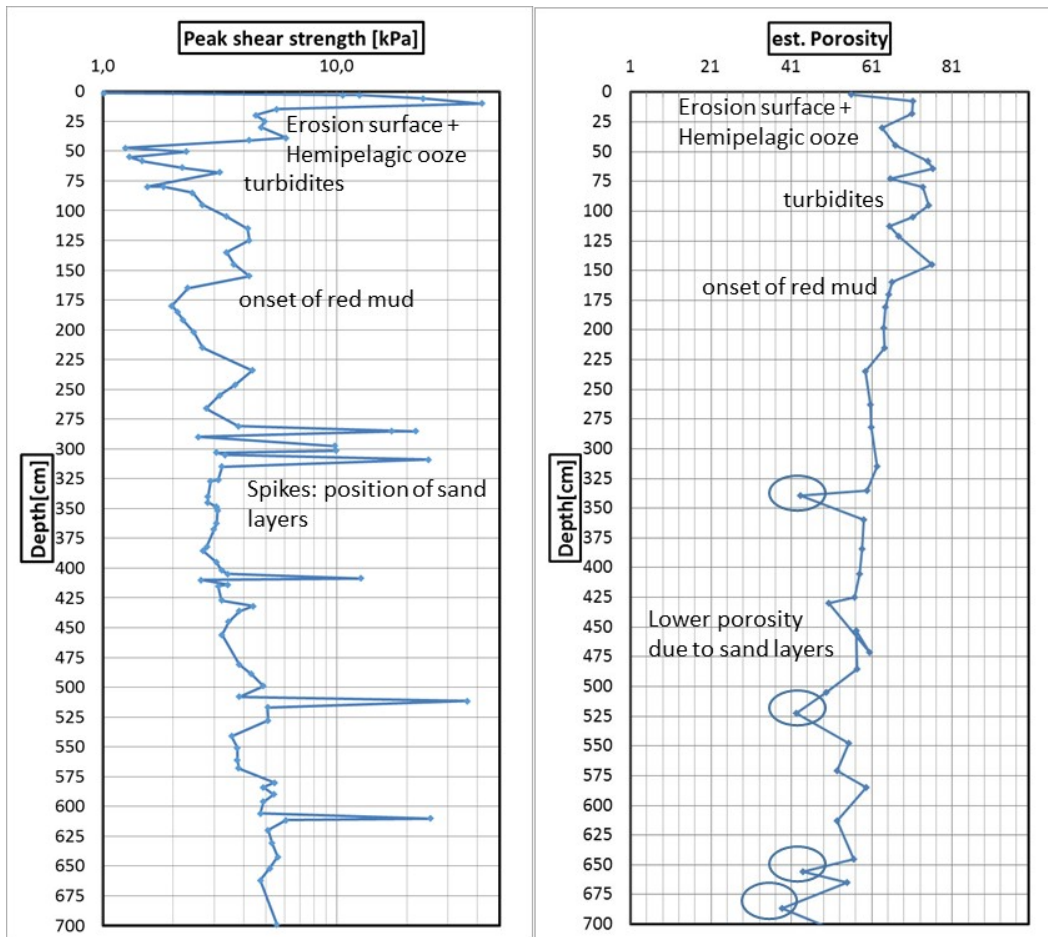


Fig. 5.22 Left: Display of averaged undrained shear strength measurements in core 13_2. The first few centimetres of sediment exhibit very low shear strength, with a marked increase at approx. 5 cm depth that corresponds to the description of very stiff hemipelagic layers close to the top of the cores. Beneath, a sequence of fine-grained turbidites shows a varied shear strength pattern. Shear strength decreases with the deposition of red mud, and increases again with depth. Spikes mark the position of sandy turbidites within the red mud. Right: Porosity measurements (estimated with a sediment grain size density of 2.7 g/cm^3 and a water density of 1.03 g/cm^3) follow the same pattern as the shear strength measurements.

Transect 4

This transect was decided on the basis of an old core (85001-15) discussed in Clarke (1988), which contains about 2 m of gravel normally grading to sand and silt. However, three out of four attempts were unsuccessful, where the corer either did not trigger (035-1) or bounced (gravity cores 036-1 and 036-2). Gravity core 037-1 did however retrieve 44 cm

of gravel from the right-channel margin about 30 m above the channel thalweg in hummocky PARASOUND acoustic character.

Transect 5

This transect was taken from the Western Valley and links with transect 2 at Core 013. Two cores, one at the thalweg (GBC 034-1) at similar backscatter signature as the southern branch thalweg core (031) and one 70 m above the channel thalweg (GC 033-1), both retrieved very fluid turbidite muds. Core 034-1, taken in the thalweg, had 20 cm of mud on top of very fluid fine sand, which was resting on top of very compacted sand.

5.4 CPT measurements

(R. Roskoden, L. Mehringer, M. Lange)

On MSM47, we used the MARUM deep-water free-fall cone penetrating testing (CPT) probe to conduct measurements of the geotechnical properties of initial and post-failure sediments along the St. Pierre Slope (Fig. 5.3). CPT is an effective method for measuring *in-situ* physical parameters of the uppermost sediments by means of cone resistance and pore pressure (Lunne et al. 1997). These parameters can then be used to calculate geotechnical parameters such as undrained shear strength and sensitivity, which are essential for estimating slope stability.

5.4.1 Instrumentation

The dynamic deep-water penetrometer measures two different parameters (Fig. 5.23):

1. The resistance at the cone shaped tip (with an area of 15 cm²), called '*cone resistance*' (q_c) in [kPa], measured via strain gauges inside the probe.
2. The *pore pressure* (u) [kPa] at three locations u_1, u_2, u_3 .

The pore pressure is measured via differential pressure sensors. Two out of three pore pressure locations can be used simultaneously, allowing short and long-term dissipation testing in two different depths and therefore possibly two different sediment types. The maximal capacity of the pore pressure sensors is restricted to 10 MPa. The data acquisition can be monitored directly via an integrated telemetry cable and a custom communication tool. The pore pressure ports are connected to valves allowing the user to bypass the sensors and thereby resetting the pore pressure measurements in case the maximum capacity is exceeded. The CPT has a waterproofed housing that hosts the power supply, the pore pressure tubing and the electronics like volatile memory, microprocessors, sensors as well as a communication box for downloading the data. The housing tolerates 30 MPa confining pressures. Hence, the CPT can be operated in water depth down to 3000 m. Two non-volatile battery packs provide performance times of about six to twelve hours, respectively.

Frequency of data acquisition is 1000 Hz. Binary data are temporarily stored on a Micro Flash Card and then downloaded to a PC via a wireless connection. The length of the lance for this cruise was 213 cm. The weight of the instrument was ca. 350 kg. After penetrating the subsurface, the instrument remained in the seafloor for about 20 minutes for short-term semi-dissipation tests. Besides the above-mentioned measurements (Fig. 5.23), the CPT includes also two inclinometers, installed at the upper part of the housing, which monitor the penetration angle up +/-20° relative to vertical.

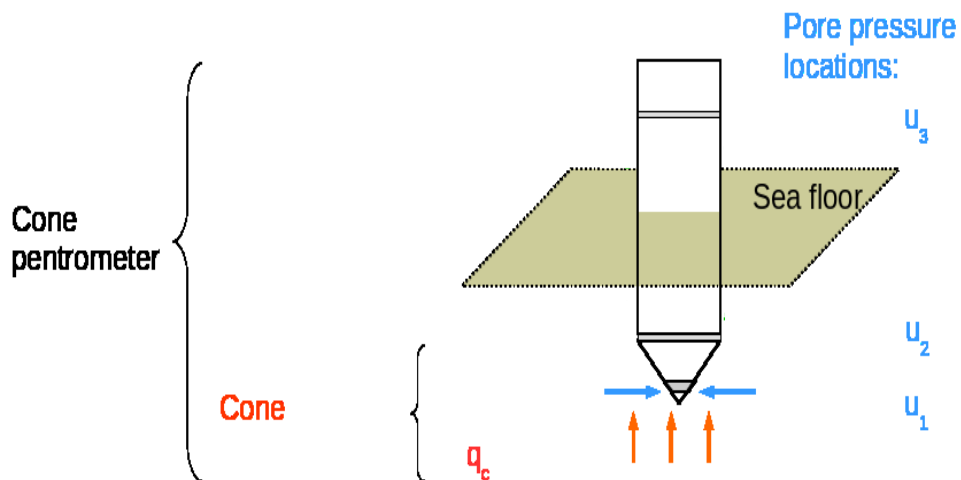


Fig. 5.23 CPT nomenclature, the cone penetrometer with the cone at the tip. The pore-water pressure can be measured at three different places u_1 to u_3 . The forces acting on the different parts of the penetrometer are indicated with arrows in different colors.

Furthermore, five different accelerometers provide information about the measured de-/acceleration of the instrument during penetration. They range of the accelerometers differs ($+/- 1.7g$, $+/- 18g$, $+/- 32g$, $+/- 50g$, $+/- 120g$) in order to guarantee best possible data over a wide range. The penetration velocity and depth is approximated via cumulative trapezoidal methods for calculating the area under the de-/ acceleration graph.

5.4.2 Data acquisition

To acquire data of undisturbed as well as post-failure sediment across the slope, the CPT measurements were taken along three transects on the St. Pierre Slope based on PARASOUND and multibeam data (Figs 029 and 5.25). A total of 18 CPT drops were conducted in the northern working area. Water depths ranged from 800 to 2000 mbsl. The penetration depth ranged from 1 to 3 mbsf. The instrument was operated in a “yo-yo-style”. The winch-velocity for penetration was set for 1 m/s, recovery from the sediment until the sediment surface was at a speed of 0.2 m/s and the vertical transect velocity was set to 1.5

m/s. Before penetration at each station, the valves of the pore pressure ports were opened and closed to calibrate the display of the penetration for the pore pressure monitoring.

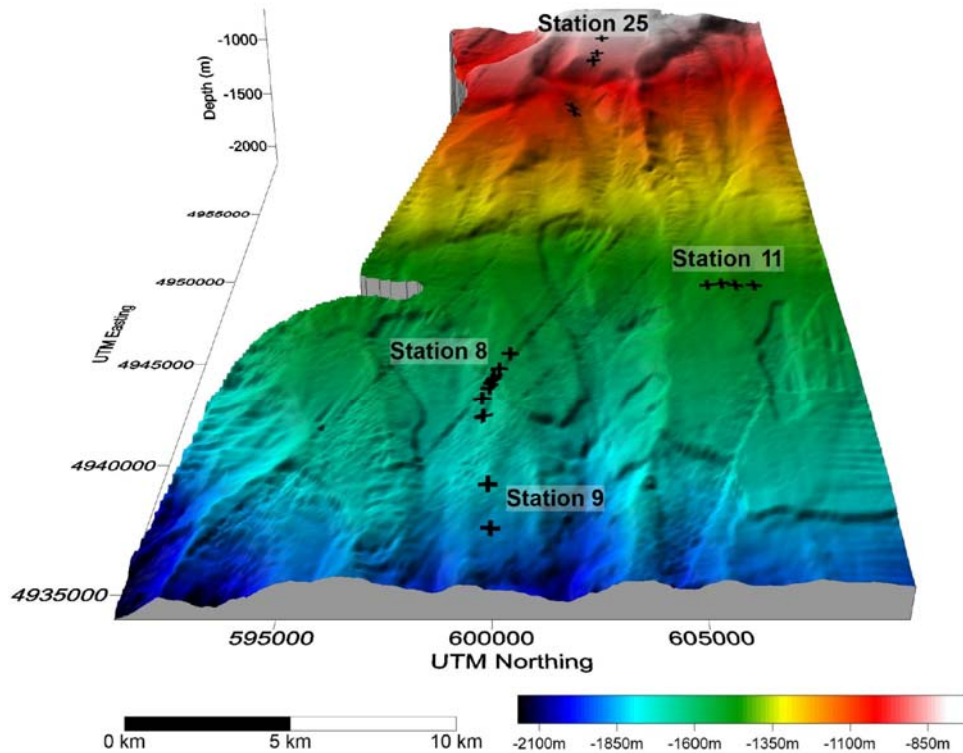


Fig. 5.24 Detailed bathymetric map (rainbow colors) of the St. Pierre Slope Area showing the morphological characteristics for the CPT measurements along three transects

Transect Station 8 and 9

This North-South transect of the middle to lower St. Pierre Slope (Figs. 029 and 5.25) includes nine penetrations, carried out in two intervals due to a low battery after Station 008_06. Two penetrations are located above a scarp (Fig. 5.25). Three penetrations are located at terraces of the scarp, followed by three additional penetrations, which are situated within slide deposits (Fig. 5.25). The last penetration (009_03) was placed in well-stratified sediment without any indication of slide deposits further downslope.

Transect Station 7 and 11

The strength of sediments were measured along an E-W transect in the middle of the St. Pierre Slope area (Figs. 023 and 029). Here, the CPT was dropped twice in an acoustically transparent sediment lens (Fig. 5.18) and one penetration on each side of the sediment lens in well stratified sediments.

Transect Station 25

This transect includes five penetrations of the CPT which were measured in downslope direction of a scarp/small headwall on the upper St. Pierre Slope (Fig. 5.24). Again, the strategy of the measurement was to place a penetration above the scarp, as well as further downslope in an area where failure may have occurred recently (025_01 to 025_04).

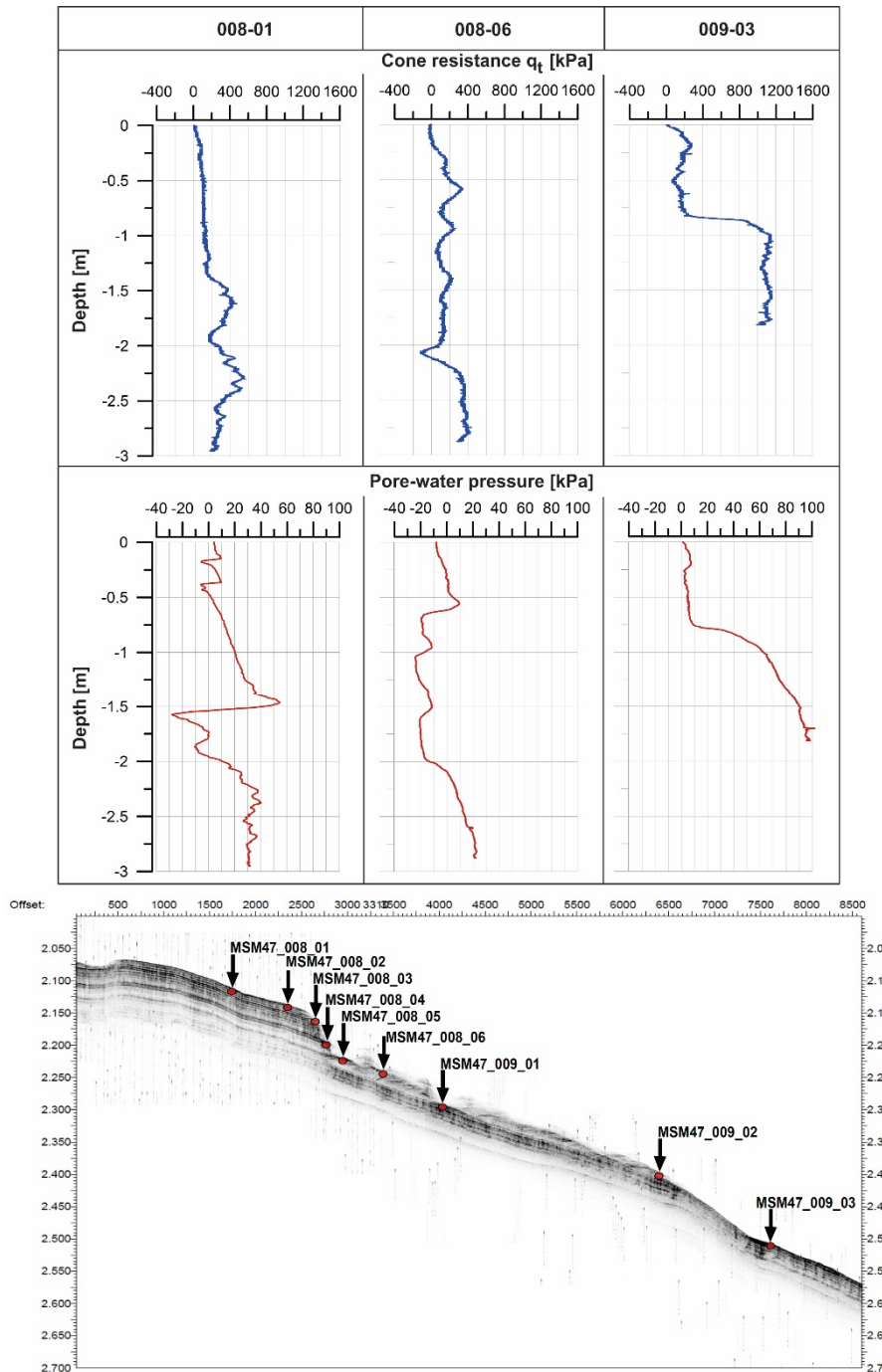


Fig. 5.25 Example for cone resistance (q_c)(upper graphs-blue) and pore-water pressure measurements (lower graphs-red) for selected stations. PARASOUND-plot for transect station 8 and 9; penetration locations marked with red dots.

The last drop of this transect (025_05) is located within the slide deposits, characterized by a chaotic, acoustically transparent PARASOUND signal. The transect was planned for 7 drops, but had to be aborted after the fifth station due to low battery, most likely caused by water leakage.

5.4.3 Data processing

Transect stations 8/9 and 7/11 were completed as planned and the processed data look promising. During transect 25, a water leakage occurred and caused the battery voltage to drop drastically, which led to abandonment of the transect after 5 stations. Unusual and most likely artificial spikes in the deceleration data make the calculation of the penetration depth difficult. To eradicate this, a frequency analysis and despiking of the data will be done during full data processing.

Table 5.2 Three examples of existing studies for SF values from (Steiner 2013)

Soil Type	SF	Reference
Remolded clay	0.3 – 1.5 and 0.38 – 0.93	(Dayal, U. and Allen, J.H., 1975)
Kaolin clay	0.1 – 0.15	(Randolph and Hope, 2004)
Clay to silt clay	0.13 to 0.45	(Steiner, A., 2013)

One file stores 900 000 CPT data points (equals 15 min of acquisition time). After cutting the data into time frames, the data are corrected for offsets and calibrated (recalculated to SI units). Penetration depth is calculated via a double integration of the deceleration. Due to the dynamic velocity of the free fall CPT, the data are influenced by the deformation rate -also called the strain rate- effects. These effects alternate the strength properties (e.g. cone resistance and sleeve friction) of the sediment. Therefore, the strength properties need to be corrected for the change in penetration velocity, which is called penetration rate correction. Corrections are based on statistically estimated formulas and the so-called strength factor, which depends on the sediment type (Dayal and Allen 1975, Randolph and Hope, 2004, Stoll et al., 2007, Stark 2010, Steiner 2013). The used values for the preliminary results refer to Steiner, A. (2013) (Table 5.2). Afterwards a geological interpretation can be done for example by calculating the mechanical soil properties like the sensitivity and the undrained shear strength.

5.4.4 Preliminary results

The de/acceleration, velocity, pore pressure and relative pore pressure and cone resistance were measured (Fig. 5.26). Pore pressure and cone resistance measurements for selected representative penetrations are shown in Fig. 5.25 for the combined Transect 8/9. Sediments above the headwall are characterized by low cone resistance and pore pressures in the first meter below the seafloor. Further down in the sediment, cone resistance shows distinct peaks (Fig. 5.25, Penetration 008-01). The upper peak coincides with a sharp

decrease in pore pressure (Fig. 5.25, Penetration 008-01). The data suggest that at least three layers with different sediment properties were penetrated. Penetrations located on terraces and in the slide mass are characterized by similar cone resistance values, which are more or less constant below 500 kPa.

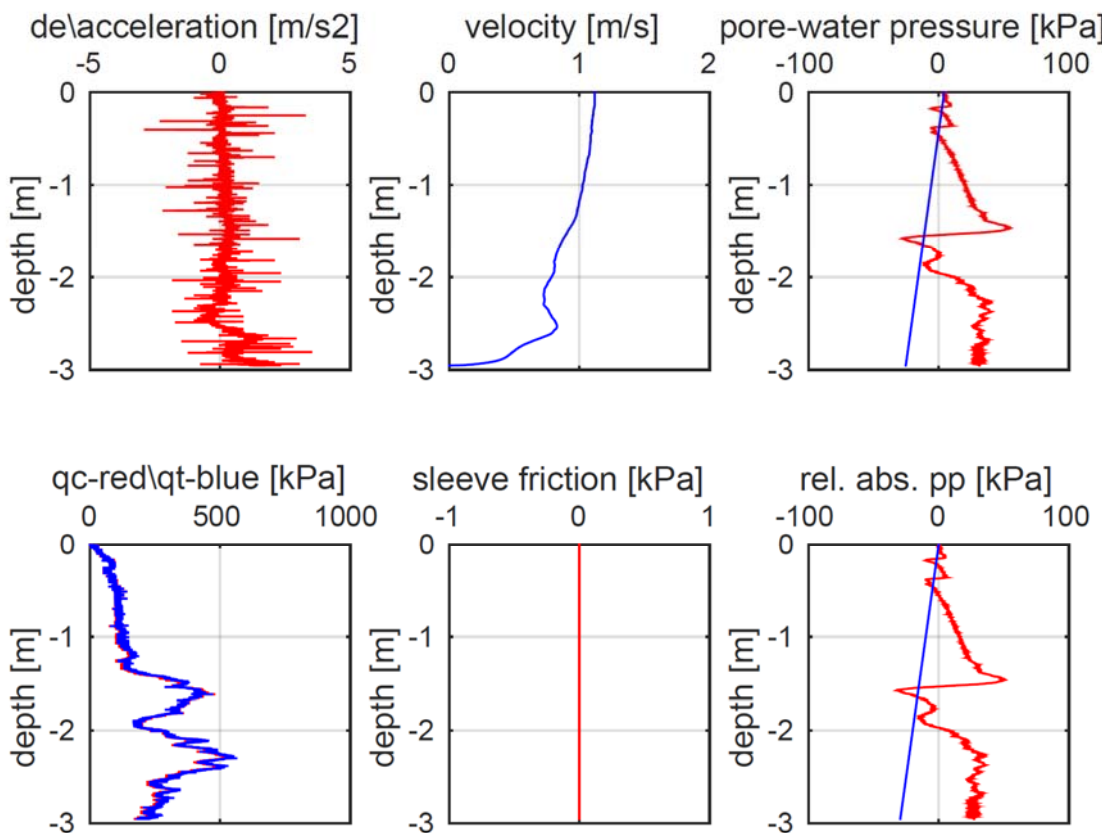


Fig. 5.26 Example for the preliminary results after processing for penetration 008-01. From upper left to the lower right: The de\ acceleration, the velocity estimated from the acceleration, the pore pressure (red) and the hydrostatic pressure (blue), the cone resistance, the sleeve friction (here 0 because not measured), and the relative pore pressure with a relative offset (red) and the hydrostatic pressure (blue).

Pore pressure values show larger variations but do not exceed 50 kPa (Fig. 5.25, Penetration 008-06) suggesting a highly variable sedimentary succession. E.g., a decrease in pore pressure would point to a more permeable and probably coarser grained sediment, while an increase in pore pressure would indicate a less permeable, finer grained sediment. Distinct peaks or troughs, however, cannot be correlated between penetrations in the slide mass, indicating disturbed sediment rather than a well-stratified sedimentary succession. This is also supported by the PARASOUND plot (Fig. 5.25), which shows a chaotic seismic facies.

In sediments below the slide mass (Fig. 5.25, Penetration 009-02), cone resistance and pore pressure increase rapidly. The penetration shown in Fig. 5.25 most likely penetrated the slide mass down to 80 cm below the seafloor, indicated by similar values of cone resistance and pore pressure as in the slide mass further upslope. The sediment below 80

cm probably represents sediment not affected by the slide, indicated by the highest cone resistances and pore pressures measured in this transect (sharp increase illustrated on figure 030, Penetration 009-02). Hence the glide plane was penetrated.

6 Ship's Meteorological Station

There was no meteorologist on board during the cruise.

7 Station List MSM47

Table 7.3 Station list including ship's and internal station number.

Stationlist RV MARIA S. MERIAN Cruise MSM47

BC: Giant Box Core, CPT: Cone Penetrating Testing, GC: Gravity Core

MB+PS: Multibeam and PARASOUND, SEISREFL: Seismic Reflection,

SVP: Sound Velocity Profile, XSV: Sippican Extended SVP

Station No.		Date	Gear	Time	Lat	Long	Water Depth	Remarks/Recovery
MERIAN MSM47	CAU, MSM 47			[UTC]	[N]	[W]	[m]	
478-1	01-1	1.10.	SVP	14:21	44°31.83'	-55°01.84'	2437	
478-1	01-2	1.10.	GC	15:48	44°31.83'	-55°01.83'	2438	overpenetration
478-1	01-3	1.10.	GC	17:55	44°31.81'	-55°01.82'	2441	810 cm recovery
478-1	01-4	1.10.	CPT	19:45	44°31.81'	-55°01.82'	2442	
479-1		1.10.	SEISREFL	21:42				see separate list
481-1	02-1	4.10.	BC	12:42	44°30.31'	-55°06.74'	3004	
482-1	03-1	4.10.	BC	15:18	44°30.46'	-55°06.11'	2948	with Posidonia
482-2	03-2	4.10.	GC (3m)	17:44	44°30.46'	-55°06.10'	2950	256 cm recovery
487-1	04-1	5.10.	BC	16:24	44°34.80'	-55°44.54'	1783	with Posidonia
487-2	04-2	5.10.	GC (11m)	18:01	44°34.81'	-55°44.53'	1782	395 cm recovery
488-1	05-1	5.10.	GC (5m)	20:08	44°37.19'	-55°44.12'	1571	overpenetration
488-2	05-2	5.10.	GC (12m)	21:26	44°37.19'	-55°44.10'	1566	787 cm recovery
488-3	05-3	5.10.	BC	22:20	44°37.19'	-55°44.10'	1566	
489-1		5.10.	SEISREFL	23:47				see separate list
490-1	06-1	6.10.	BC	13:42	44°38.71'	-55°38.72'	1487	
490-2	06-2	6.10.	GC (8m)	15:04	44°38.71'	-55°38.73'	1487	630 cm recovery
491-1	07-1	6.10.	GC (8m)	17:22	44°38.77'	-55°39.49'	1467	645 cm recovery
491-2	07-2	6.10.	CPT	19:28	44°38.77'	-55°39.48'	1467	
492-1		8.10.	MB+PS	10:10	44°31.32'	-55°44.31'	2194	several profiles
493-1	08-1	8.10.	CPT	12:43	44°37.19'	-55°44.09'	1566	
493-1	08-2	8.10.	CPT	14:15	44°36.89'	-55°44.30'	1587	
493-1	08-3	8.10.	CPT	15:15	44°36.75'	-55°44.40'	1608	
493-1	08-4	8.10.	CPT	15:56	44°36.69'	-55°44.43'	1625	
493-2		8.10.	XSV	16:24	44°36.69'	-55°44.44'	1627	
493-1	08-5	8.10.	CPT	16:57	44°36.59'	-55°44.50'	1645	
493-1	08-6	8.10.	CPT	17:57	44°36.38'	-55°44.62'	1665	
494-1		8.10.	SEISREFL	19:36	44°36.70'	-55°47.80'	1613	see separate list
495-1	09-1	9.10.	CPT	12:33	44°36.06'	-55°44.62'	1702	

Station No.		Date	Gear	Time	Lat	Long	Water Depth	Remarks/Recovery
MERIAN MSM47	CAU, MSM 47			[UTC]	[N]	[W]	[m]	
495-1	09-2	9.10.	CPT	15:04	44°34.79'	-55°44.54'	1784	
495-1	09-3	9.10.	CPT	16:34	44°34.11'	-55°44.50'	1862	
496-1		9.10.	MB+PS	17:26	44°34.21'	-55°44.55'	1851	
497-1	10-1	9.10.	BC	19:39	44°45.72'	-55°41.30'	818	
497-2	10-2	9.10.	GC (8m)	20:20	44°45.72'	-55°41.29'	821	recovery 768 cm
498-1		9.10.	MB+PS	21:16	44°45.80'	-55°40.09'	1271	
499-1	11-1	9.10.	CPT	22:26	44°38.71'	-55°38.76'	1481	
499-1	11-2	9.10.	CPT	23:46	44°38.73'	-55°39.18'	1465	
499-1	11-3	10.10.	CPT	0:51	44°38.77'	-55°39.78'	1482	
500-1		10.10.	MB+PS	2:03	44°38.97'	-55°45.57'	1476	
501-1	12-1	10.10.	BC	11:37	44°47.66'	-56°06.95'	791	
501-2	12-2	10.10.	GC (5m)	12:25	44°47.67'	-56°06.95'	792	500 cm recovery, surface may be missing
502-1		10./11.10	SEISREFL	15:50			86	see separate list
503-1		11.10.	MB+PS	17:32	43°50.30'	-55°25.87'	3433	
504-1	13-1	12.10.	BC	15:49	42°14.01'	-55°11.94'	4439	did not trigger, empty
504-2		12.10.	XSV	16:04	42°14.01'	-55°11.94'	4439	
504-3	13-2	12.10.	GC (8m)	18:59	42°14.01'	-55°11.94'	4452	recovery 775 cm
505-1		12.10.	SEISREFL	22:46				see separate list
506-1	14-1	14.10.	GC (5m)	20:43	42°02.933'	-54°22.99'	4909	no recovery
507-1		15.10.	MB+PS	0:58	42°03.35'	-54°22.68'	4904	
508-1	15-1	15.10.	GC (10m)	12:20	42°11.98'	-54°24.18'	4705	recovery 563cm
509-1		15.10.	MB+PS	15:13	42°11.96'	-54°24.23'	4869	
510-1	16-1	15.10.	BC	18:19	42°26.69'	-54°58.16'	4449	
510-2	16-2	15.10.	GC (10m)	21:28	42°26.60'	-54°58.17'	4447	recovery 597cm
511-1		16.10.	MB+PS	0:13	42°32.86'	-55°04.25'	4425	
512-1	17-1	16.10.	GC (10m)	11:45	42°41.57'	-55°01.68'	4503	no recovery
513-1	18-1	16.10.	GC (10m)	14:48	42°46.91'	-55°02.93'	4412	recovery 791 cm
514-1	19-1	16.10.	GC (10m)	17:24	42°43.09'	-55°02.02'	4481	recovery 190 cm
515-1	20-1	16.10.	GC (10m)	22:08	42°25.05'	-55°27.72'	4159	recovery 770 cm
516-1		17.10.	SEISREFL	0:36				see separate list
517-1		17.10.	MB+PS	17:25	42°53.68'	-55°44.35'	3698	
518-1		17.10.	XSV	18:36	43°00.74'	-55°37.36'	4209	
517-1		17.10.	MB+PS	20:34	43°02.51'	-55°12.48'	4262	

Station No.		Date	Gear	Time	Lat	Long	Water Depth	Remarks/Recovery
MERIAN MSM47	CAU, MSM 47			[UTC]	[N]	[W]	[m]	
519-1		18.10.	SEISREFL	12:11			3504	see separate list
520-1	21-1	19.10.	BC	9:06	42°19.70'	-55°04.29'	4653	did not trigger, empty
520-2	21-2	19.10.	GC (5m)	12:23	42°19.76'	-55°04.25'	4641	recovery 395cm
521-1	22-1	19.10.	GC (5m)	15:11	42°18.42'	-55°04.23'	4713	bent, two subsample from CC
522-1		19.10.	MB+PS	17:41	42°18.46'	-55°04.19'	4706	
523-1	23-1	20.10.	GC (10m)	10:09	44°42.82'	-55°42.67'	1114	recovery 660 cm
524-1	24-1	20.10.	GC (10m)	11:47	44°45.70'	-55°41.42'	825	recovery 337 cm
525-1	25-1	20.10.	CPT	13:06	44°45.69'	-55°41.42'	828	
525-1	25-2	20.10.	CPT	14:42	44°45.18'	-55°41.58'	870	
525-1	25-3	20.10.	CPT	15:30	44°44.99'	-55°41.69'	899	
525-1	25-4	20.10.	CPT	16:58	44°43.72'	-55°42.37'	1070	
525-1	25-5	20.10.	CPT	18:04	44°43.28'	-55°42.53'	1086	
526-1	26-1	20.10.	BC	20:25	44°44.70'	-55°38.00'	1054	
526-2	26-2	20.10.	GC(10m)	21:22	44°44.69'	-55°38.02'	1051	recovery 704 cm
527-1	04-3	20.10.	GC (5m)	23:16	44°34.80'	-55°44.36'	1786	recovery 337 cm
528-1	27-1	21.10.	GC (5m)	8:04	43°20.42'	-55°19.42'	3975	no recovery
529-1	28-1	21.10.	GC (5m)	10:23	43°20.48'	-55°18.43'	3947	recovery 480cm
530-1	27-2	21.10.	BC	12:05	43°20.47'	-55°18.43'	3946	
531-1		21.10.	SEISREFL	15:49				see separate list
532-1	29-1	22.10.	GC (3m)	13:20	42°18.86'	-55°03.90'	4669	no recovery
533-1		22.10.	MB+PS	15:22	42°18.87'	-55°03.93'	4670	
534-1	30-1	22.10.	GC (3m)	16:58	42°15.43'	-55°09.59'	4577	recovery 290cm
535-1	31-1	22.10.	BC	19:26	42°16.80'	-55°07.45'	4814	
536-1	32-1	22.10.	BC	23:07	42°15.92'	-55°08.79'	4661	
537-1	31-2	23.10.	GC (3m)	2:30	42°16.79'	-55°07.46'	4813	recovery 40 cm
538-1		23.10.	SEISREFL	5:23				see separate list
539-1		23.10.	MB+PS	14:30	42°19.05'	-55°58.70'	4151	
540-1	33-1	23.10.	GC (3m)	17:30	42°16.25'	-55°34.53'	4505	recovery ~ 150 cm
541-1	34-1	23.10.	BC	20:00	42:15.48'	-55°39.17'	4608	
542-1		23.10.	MB+PS	23:24	42°15.49'	-55°39.32'	4603	
543-1		24.10.	XSV	16:12	41°32.57'	-53°47.27'	4933	
542-1		24.10.	MB+PS	17:23	41°25.45'	-53°42.58'	4970	
544-1	35-1	24.10.	BC	23:28	41°22.25'	-53°34.20'	5037	
545-1	36-1	25.10.	GC (5m)	3:38	41°17.31'	-53°38.00'	5016	no recovery

Station No.		Date	Gear	Time	Lat	Long	Water Depth	Remarks/Recovery
MERIAN MSM47	CAU, MSM 47			[UTC]	[N]	[W]	[m]	
546-1	37-1	25.10.	GC (5m)	6:21	41°20.13'	-53°35.80'	5012	recovery 45cm
547-1	36-2	25.10.	GC (5m)	9:16	41°17.32'	-53°38.02'	5012	no recovery
548-1		25.10.	MB+PS	11:40	41°17.32'	-53°37.99'	5017	

Table 7.4: List of seismic profiles.

Profil-Nr. GeoEEL MSM47	Date	Time Start UTC	Time End UTC	Latitude Start N	Lon Start W	Latitude End N	Lon End W	Geom. Start FFN Start	Geom. End FFN End
001	1./2.10	23:51	02:45	44°25.57'	54°59.92'	44°13.73'	54°52.08'	567	2007
002	2.10.	05:34	09:27	44°12.45'	54°56.28'	44°08.37'	55°17.01'	3003	5005
003	2.10.	11:10	20:50	44°8.84'	55°15.10'	43°57.33'	56°12.95'	5500	10482
004	2.10.	21:42	21:58	43°56.3'82	56°17.78'	43°56.12'	56°19.08'	11000	11138
005	2./3.10	22:40	02:25	43°55.80'	56°21.46'	43°51.64'	56°41.22'	11263	13207
006	3.10.	02:37	06:57	43°52.15'	56°41.73'	44°09.47'	56°41.84'	13297	15536
007	3.10.	07:32	08:47	44°11.74'	56°41.83'	44°16.60'	56°41.82'	16000	16745
008	3.10.	08:56	22:33	44°16.94'	56°41.24'	44°33.08'	55°28.95'	16845	25018
009	3./4.10	22:34	03:00	44°33.19'	55°28.69'	44°42.59'	55°06.19'	25019	27679
010	4.10.	03:10	07:01	44°42.04'	55°05.22'	44°25.09'	54°59.26'	27788	30107
011	6.10.	00:23	00:41	44°36.75'	55°41.04'	44°36.53'	55°39.40'	31000	31212
012	6.10.	00:51	02:53	44°35.96'	55°39.00'	44°26.75'	55°39.05'	31311	32525
013	6.10.	03:01	03:36	44°26.41'	55°38.40'	44°26.34'	55°34.68'	32608	32958
014	6.10.	03:45	04:11	44°27.08'	55°34.15'	44°28.09'	55°33.99'	33044	33286
015	6.10.	04:26	08:16	44°29.85'	55°33.91'	44°47.07'	55°32.85'	33400	35709
016	6.10.	08:25	09:05	44°47.57'	55°33.30'	44°48.37'	55°37.11'	35794	36180
017	6.10.	09:11	11:56	44°48.02'	55°37.59'	44°35.78'	55°39.05'	36245	37896
018	8.10.	19:33	22:28	44°36.90'	55°47.72'	44°23.18'	55°50.92'	38073	39518
019	8./9.10	22:40	03:53	44°23.06'	55°49.79'	44°30.26'	55°17.64'	39952	43076
020	9.10.	04:00	05:22	44°30.05'	55°16.87'	44°24.20'	55°14.26'	43150	43967
021	9.10.	05:33	09:08	44°23.53'	55°14.85'	44°19.20'	55°36.55'	44080	46229
022	9.10.	09:20	10:58	44°19.61'	55°37.37'	44°26.75'	55°39.05'	46348	47309
023	9.10.	10:59	11:09	44°26.90'	55°39.06'	44°27.62'	55°39.06'	47322	47427
024	10.10.	15:45	22:57	45°02.76'	55°48.02'	44°33.48'	55°41.26	48000	53168
025	10./11. 10	23:06	01:12	44°33.46'	55°40.86'	44°37.08'	55°29.04	53291	54802
026	11.10.	01:19	8:20	44°37.16'	55°28.36'	44°09.42'	55°13.04	54883	58758
027	11.10.	8:30	11:51	44°08.84'	55°13.23'	43°57.07'	55°24.21	58832	60324
028	11.10.	12:25	15:13	43°57.61'	55°23.96'	43°45.99'	55°21.70	60336	61584
029	12./13. 10	22:51	8:27	42°10.43'	55°21.21'	42°45.40'	54.46.88	62000	66074
030	13.10.	8:37	10:40	42°45.53'	54°46.07'	42°39.20'	54°37.08	66140	67009
031	13.10.	10:44	20:00	42°39.91'	54°36.99'	41°58.99'	54.51.22	67045	70934
032	13.10.	20:03	22:15	41°58.55'	54°50.95'	41°52.89'	54°40.16	70981	71911

Profil-Nr. GeoEEL	Date	Time Start UTC	Time End UTC	Latitude Start N	Lon Start W	Latitude End N	Lon End W	Geom. Start FFN Start	Geom. End FFN End
MSM47									
033	13./14. 10	22:22	8:05	41°52.90'	54°39.43'	42°30.40'	54°09.50	71963	76082
034	14.10.	8:12	9:23	42°30.56'	54°08.88'	42°26.97'	54°03.59	76127	76632
035	14.10.	9:30	18:36	42°26.52'	54°03.39'	41°46.07'	54°09.06	76679	80535
036	16./17. 10	1:37	8:59	42°29.28'	55°34.61'	42°51.65'	55°00.36	81205	84328
037	17.10.	9:06	10:13	42°52.08'	55°00.06'	42°57.05'	55°02.11	84377	84840
038	17.10.	10:21	16:47	42°57.12'	55°02.62'	42°53.94'	55°42.06	84904	87647
039	18.10.	12:47	15:29	43°46.62'	55°21.78'	43°34.58'	55°19.96	88065	89369
040	18.10.	15:33	20:41	43°34.33'	55°19.81'	43°16.16'	55°00.15	89395	91758
041	18./19. 10	20:46	6:52	43°15.89'	54°59.99'	42°30.43'	55°00.00	91790	96075
042	21./22. 10	18:59	0:32	43°20.89'	55°25.59'	43°13.02'	54°51.58	97212	99558
043	22.10.	0:41	1:17	43°18.48'	54°51.14'	43°15.87'	54°51.05	99630	99880
044	22.10.	1:24	3:27	43°15.49'	54°51.43'	43°10.72'	55°02.29	99929	100806
045	22.10.	3:31	7:56	43°10.65'	55°02.49'	43°05.38'	55°27.77	100828	102699
046	23.10.	5:54	13:13	42°14.44'	55°15.87'	42°12.88'	55°59.42	103041	106142

Table 7.5: List of CPT stations

1 CPTU had to be retrieved on deck due to low battery

2 continuation of transect 1

3 CPTU had to be retrieved on deck due to low battery, transect was not continued

Station No.		Date	Time	Latitude	Longitude	Water Depth	rope length	Remarks
MERIAN	CAU	2015	[UTC]	[N]	[W]	[m]	[m]	
MSM47_49 3-0001	MSM47_008-01	08.10.	13:12	44° 37.198'	55° 44.084'	1565	1577	
MSM47_49 3-0001	MSM47_008-02	08.10	14:16	44° 36.887'	55° 44.287'	1587		
MSM47_49 3-0001	MSM47_008-03	08.10	15:15	44° 36.747'	55° 44.394'	1606		
MSM47_49 3-0001	MSM47_008-04	08.10	16:01	44° 36.688'	55° 44.435'	1627		
MSM47_49 3-0001	MSM47_008-05	08.10	16:58	44° 36.599'	55° 44.492'	1646	1636	
MSM47_49 3-0001	MSM47_008-06	08.10	17:57	44° 36.390'	55° 44.624'	1664	1657	*1
MSM47_49 5-0001	MSM47_009-01	09.10	13:01	44° 36.048'	55° 44.606'	1700	1692	*2
MSM47_49 5-0001	MSM47_009-02	09.10	15:01	44° 34.792'	55° 44.537'	1787	1777	
MSM47_49 5-0001	MSM47_009-03	09.10	16:34	44° 34.120'	55° 44.499'	1861	1852	
MSM47_49 1-0002	MSM47_007-02	09.10	19:57	44° 38.771'	55° 39.481'	1470		
MSM47_49 7-0002	MSM47_011-01	09.10	22:48	44° 38.765'	55° 38.765'	1482	1473	
MSM47_49 7-0002	MSM47_011-02	09.10	23:46	44° 38.735'	55° 39.170'	1467	1451	
MSM47_49 7-0002	MSM47_011-03	09.10	0:52	44° 38.770'	55° 39.771'	1480	1470	
MSM47_52 5-0001	MSM47_025-01	10.10	13:24	44° 45.723'	55° 41.413'	827	816	
MSM47_52 5-0001	MSM47_025-02	20.10	14:42	44° 45.189'	55° 41.574'	873	860	
MSM47_52 5-0001	MSM47_025-03	20.10	15:30	44° 44.999'	55° 41.689'	900	889	
MSM47_52 5-0001	MSM47_025-04	20.10	16:58	44° 43.718'	55° 42.363'	1070	1059	
MSM47_52 5-0001	MSM47_025-05	20.10	18:07	44° 43.536'	55° 42.292'	1084	1075	*3

8 Data and Sample Storage and Availability

All meta-data of the cruise were made available immediately after the cruise via the Kiel data portal for marine science (<https://portal.geomar.de/metadata/leg/show/333156>). The seismic, bathymetric and hydro-acoustic raw data as well as processed seismic data are archived on a dedicated server at Kiel University. The acoustic data will be submitted to a public data base as soon as such a data base for long-term archival will be available and standards for archiving have been defined. The moratorium for exclusive use by MSM47 scientists is set to three years until November 1st, 2018. Thereafter the data will be available for other scientists upon request.

All cores are stored and archived in the Kiel core repository. The MSM47 scientific party has a three-year moratorium time until November 1st, 2018, for exclusive analytical work before the cores will be available for sampling by other scientists upon reasonable statement. All data measured at the cores during the cruise and post cruise will be included in the PANGAEA data base in Bremerhaven, which will then provide long-term archival and access to the data within WDC-MARE.

Table 8.6

Type	Database	Available	Free access	Contact
Hydrography Raw data CTD, ADCP	BSH	Oct. 2015	Nov. 2018	skrastel@geophysik.uni-kiel.de
Seismics MCS	Local	Oct. 2015	Nov. 2018	skrastel@geophysik.uni-kiel.de
Parasound	Local	Oct. 2015	Nov. 2018	skrastel@geophysik.uni-kiel.de
Sedimentology Gravity cores Box Corer	Pangaea Pangea	Jan. 2017 Jan. 2017	Nov. 2018 Nov. 2018	peter.feldens@io-warnemünde.de peter.feldens@io-warnemünde.de

9 Acknowledgements

The scientific party of Cruise MSM47 gratefully acknowledges the very friendly and most effective cooperation with Captain Schmidt and his crew. Their perfect technical assistance and great flexibility made this cruise a scientific success. We also appreciate the valuable support by the Leitstelle Deutsche Forschungsschiffe at the University of Hamburg. This expedition was funded by the Deutsche Forschungsgemeinschaft (DFG) and the Bundesministerium für Bildung und Forschung (BMBF).

10 References

- Bent, A.L., 1995. A Complex Double-Couple Source Mechanism for the Ms 7.2 1929 Grand Banks Earthquake. *Bulletin of the Seismological Society of America*, 85, 1003-1020.
- Clarke, J.E.H., 1988. The Geological Record of the 1929" Grand Banks" Earthquake and Its Relevance to Deep-Sea Clastic Sedimentation. PhD Thesis, Dalhousie University.
- Clarke, J.E.H., Shor, A.N., Piper, D.J.W., Mayer, L.A. 1990. Large-Scale Current-Induced Erosion and Deposition in the Path of the 1929 Grand Banks Turbidity Current. *Sedimentology*, 37, 613-629.
- Dayal, U., Allen, J.H., 1975. The Effect of Penetration Rate on the Strength of Remolded Clay and Sand Samples. *Canadian Geotechnical Journal*, 12, 336-348.
- Harbitz, C.B., Løvholt, F. & Bungum, H., 2014. Submarine Landslide Tsunamis: How Extreme and How Likely? *Natural Hazards*, 72, 1341-1374.
- Krastel, S., Behrmann, J.-H., Völker, D., Stipp, M., Berndt, C., Urgeles, R., Chaytor, J., Huhn, K., Strasser, M., Harbitz, C.B., 2014. Submarine Mass Movements and Their Consequences. 6th International Symposium. Springer, *Advances in Natural and Technological Hazard Research*.
- Lamarche, G., Mountjoy, J., Bull, S., Hubble, T., Krastel, S., Lane, E., Micallef, A., Moscardelli, L., Mueller, C., Pecher, I., Woelz, S., 2016. Submarine Mass Movements and Their Consequences. 7th International Symposium. Springer, *Advances in Natural and Technological Research*.
- Lunne, T., Robertson, P., Powell, J.J.M., 1997. Cone Penetration Testing.
- Mosher, D., Moscardelli, L., Shipp, R., Chaytor, J., Baxter, C., Lee, H., Urgeles, R., 2010. Submarine Mass Movements and Their Consequences, 4th International Symposium. Springer, *Advances in Natural and Technological Hazard Research*.
- Mosher, D.C., 2009. International Year of Planet Earth 7. Oceans: Submarine Landslides and Consequent Tsunamis in Canada. *Geoscience Canada*, 36.
- Randolph, M. & Hope, S., 2004. Effect of Cone Velocity on Cone Resistance and Excess Pore Pressures. Proc., Int. Symp. on Engineering Practice and Performance of Soft Deposits, Japanese Geotechnical Society Tokyo.
- Stark, N., 2010. Geotechnical Investigation of Sediment Remobilization Processes Using Dynamic Penetrometers, PhD Thesis, Bremen University, Bremen.

- Steiner, A., 2013. Sub-Seafloor Characterization and Stability of Submarine Slope Sediments Using Dynamic and Static Piezocene Penetrometers. PhD Thesis, Bremen University, Bremen.
- Stoll, R.D., Sun, Y.-F. & Bitte, I., 2007. Seafloor Properties from Penetrometer Tests. Oceanic Engineering, IEEE Journal of, 32, 57-63.
- Tappin, D., Watts, P., McMurtry, G., Lafoy, Y. & Matsumoto, T., 2001. The Sissano, Papua New Guinea Tsunami of July 1998 - Offshore Evidence on the Source Mechanism. Marine Geology, 175, 1-23.
- Tappin, D., Watts, P. & Grilli, S., 2008. The Papua New Guinea Tsunami of 17 July 1998: Anatomy of a Catastrophic Event. Natural Hazards and Earth System Sciences, 8, 243-266.
- Yamada, Y., Kawamura, K., Ikehara, K., Ogawa, Y., Urgeles, R., Mosher, D., Chaytor, J., Strasser, M., 2012. Submarine Mass Movements and Their Consequences. 5th International Symposium. Springer, Advances in Natural and Technological Hazard Research.